

# **Development and Analysis of Doped Alumina Ceramics for High-Performance Microwave Resonators**

## **A PROJECT REPORT**

*Submitted by*

**SAKSHI GHULE (112111018)**

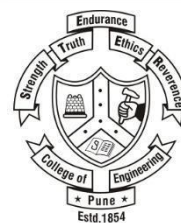
**TANISHKA PADALKAR (112111041)**

*In partial fulfillment for the award of the degree of*

**BACHELOR OF TECHNOLOGY**

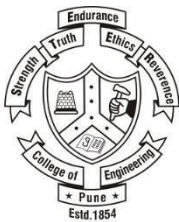
**IN**

**METALLURGY AND MATERIAL TECHNOLOGY**



**COLLEGE OF ENGINEERING, PUNE – 411005**

**MAY 2025**



DEPARTMENT OF METALLURGY  
AND MATERIAL ENGINEERING  
COLLEGE OF ENGINEERING, PUNE 411005 (INDIA)

## CERTIFICATE

This is certified that the project report “Development and Analysis of Doped Alumina Ceramics for High-Performance Microwave Resonators ” is the bonafide work of “**SAKSHI GHULE AND TANISHKA PADALKAR**” who carried out the project work under my guidance.

SIGNATURE

**Dr. M. G. Kulthe.**

**HEAD OF DEPARTMENT**

Metallurgy and Material Engineering,  
College of Engineering, Pune-411005

SIGNATURE

**Dr. S .P . Butee.**

**PROJECT GUIDE  
Professor**

Metallurgy and Material Engineering,  
College of Engineering, Pune-411005

# APPROVAL SHEET

*This report entitled.*

## **Development and Analysis of Doped Alumina Ceramics for High-Performance Microwave Resonators**

By

**Sakshi Ghule (112111018)**

**Tanishka Padalkar (112111041)**

*is approved for the degree of*

**BACHELOR OF TECHNOLOGY**

*of*

**METALLURGY AND MATERIAL SCIENCE ENGINEERING**

**College of Engineering, Pune  
(An autonomous institute of Govt. of Maharashtra)**

**Examiner**

**Name**

**Signature**

**1. External Examiner** \_\_\_\_\_

**2. Internal Examiner** \_\_\_\_\_

**3. Supervisor** \_\_\_\_\_

**Date:**

**Place:**

## TABLE OF CONTENTS

<b>CHAPTER NO</b>	<b>TITLE</b>	<b>PAGE NO</b>
	<b>TABLE OF CONTENTS</b>	3
	<b>LIST OF FIGURES</b>	5
	<b>ABSTRACT</b>	6
<b>1.</b>	<b>INTRODUCTION</b>	7
<b>2.</b>	<b>LITERATURE REVIEW</b>	9
2.1	Dielectric Resonator	9
2.2	Materials	11
2.3	Post Processing	16
2.3.1	Sintering	16
2.3.2	Dielectric Testing	18
2.3.3	Mechanical Testing	22
<b>3.</b>	<b>EXPERIMENTAL WORK</b>	24
3.1	Material Selection	24
3.2	Sample Preparation	25
3.2.1	Powder Weighing and Dopant addition	25
3.2.2	Mixing and Binder addition	26
3.2.3	Pellets Formation (Hydraulic Press)	27
3.2.4	Drying and Debinding	27
3.3	Sintering Procedure	28
3.4	Surface Polishing	30
3.5	Dielectric Characterization by using VNA	32
3.6	Impedance Spectroscopy	33
3.7	Mechanical Testing	34
3.8	XRD Testing	36
<b>4.</b>	<b>RESULT AND DISCUSSION</b>	38
4.1	XRD	38
4.2	Dielectric Testing	40
4.2.1	Bode Plot	40
4.2.2	Dielectric Constant- Impedance Spectroscopy	41
4.2.3	Dielectric Loss- Impedance Spectroscopy	44

4.2.4	Dielectric Constant-VNA	46
4.2.5	Dielectric Loss-VNA	50
4.3	Hardness Test	52
4.4	Compression Test	
<b>5.</b>	<b>CONCLUSIONS</b>	56
<b>6.</b>	<b>FUTURE SCOPE</b>	57
	<b>REFERENCES</b>	58
	<b>Acknowledgement</b>	59

## LIST OF FIGURES

No.	Description
1	Dielectric Resonator
2	Binder Preparation Setup
3	Stages of Sintering
4	Sintering Mechanism
5	XRD Mechanism
6	Rockwell Superficial Hardness Tester
7	Compression test
7	Material Selection
8	Mortar Pestle (mixing)
9	Hydraulic Press
10	pellets
11	Hot Oven Drying
12	Muffle Furnace
13	Pellets after Sintering
14	VNA Experimental Setup
15	Dielectric Testing Experimental setup
16	Rockwell Superficial Hardness Tester
17	XRD
18	XRD Analysis
19	Bode Analysis
20	Dielectric Constant Vs Frequency(Hz)
21	Dielectric Loss Vs Frequency(Hz)
22	FWHM
23	Dielectric Constant Vs Frequency(Hz) [VNA] of Pure Alumina, V <sub>2</sub> O <sub>5</sub> , Fe <sub>2</sub> O <sub>3</sub>
24	Dielectric Constant Vs Frequency(Hz) [VNA] of Cr, Fe <sub>2</sub> O <sub>3</sub> + TiO <sub>2</sub>
25	Dielectric Loss Vs Frequency(Hz) [VNA]
26	Hardness Analysis
27	Compression Analysis

## **LIST OF TABLES**

No.	Description
1	Properties and applications of dopants
2	Materials with its properties and applications
3	Composition of each material
4	Density measurement
5	Value of Z' w.r.t Frequency(Hz)
6	Dielectric constant value at $10^3$ Hz
7	Tangent loss value of sample w.r.t Frequency(Hz)
8	Effect of each dopant on tangent loss
9	Highest peak frequency and FWHM of samples
10	$\epsilon'$ , $\epsilon''$ , tan $\delta$ , Quality factor (loaded) values
11	Hardness values of each sintering cycle(Superfacial Rockwell machine(HR))
12	Peak Load (N) values for each sintering cycle

## **ABSTRACT.**

Alumina ( $\text{Al}_2\text{O}_3$ ) ceramics are widely used in high-frequency applications due to their superior thermal stability, mechanical strength, and moderate dielectric properties. However, the inherent dielectric loss limits their effectiveness in advanced microwave dielectric resonator devices. This project aims to optimize the dielectric and structural performance of alumina ceramics by doping them with selected transition metal oxides—namely ferric oxide ( $\text{Fe}_2\text{O}_3$ ), chromium oxide ( $\text{Cr}_2\text{O}_3$ ), a combination of ferric oxide and titanium dioxide ( $\text{Fe}_2\text{O}_3 + \text{TiO}_2$ ), and vanadium pentoxide ( $\text{V}_2\text{O}_5$ ). Each composition of  $\text{Al}_{1.9}\text{M}_{0.1}\text{O}_{3+\delta}$  ( $\text{M} = \text{Cr}, \text{V}, \text{Fe}, \text{Fe} + \text{Ti}$ ) was synthesized in three sintering cycles at  $1575^\circ\text{C}/4$  h to investigate the influence of thermal treatment. Samples were analyzed using X-ray diffraction (XRD), dielectric testing, and vector network analysis (VNA). Mechanical characterization, including microhardness and compression tests, was done. The results are expected to identify the optimal dopant and sintering condition for enhancing the dielectric properties of alumina ceramics, thereby advancing their application in microwave resonator technologies.

# **CHAPTER - 1**

## **INTRODUCTION**

In recent decades, the demand for compact, high-performance electronic components has surged, particularly in fields such as wireless communication, radar systems, and satellite technologies. Among these components, microwave dielectric resonators play a critical role in filtering, frequency selection, and signal stabilization. These resonators operate by storing electromagnetic energy at microwave frequencies and require materials with very specific dielectric properties—high dielectric constant, low dielectric loss, excellent thermal stability, and mechanical strength. The rapid advancement of wireless communication technologies has necessitated the development of high-performance microwave components that are efficient, compact, and reliable. Among these, microwave dielectric resonators are integral elements used in filters, oscillators, and antennas due to their ability to store and stabilize microwave energy with minimal loss. These devices demand materials with specific properties, such as a high dielectric constant, low dielectric loss, mechanical durability, and thermal stability.[1]

Alumina ( $\text{Al}_2\text{O}_3$ ) is one of the most widely studied ceramic materials in dielectric applications due to its excellent electrical insulation, chemical stability, high thermal conductivity, and good mechanical strength. While pure alumina already demonstrates favorable dielectric properties, it may fall short in terms of tunability and performance under demanding conditions such as high-frequency resonance or elevated temperatures. This creates an opportunity for enhancement through microstructural engineering, particularly by doping.

Numerous studies have explored the impact of dopants on alumina. According to Dong Zhao,  $\text{Fe}_2\text{O}_3$  doping can increase grain boundary conductivity while also modifying the dielectric constant and loss tangent.  $\text{Cr}_2\text{O}_3$  has been shown to improve densification and mechanical hardness while slightly reducing dielectric losses [2].  $\text{TiO}_2$  and Fe co-doping is known to enhance dielectric permittivity due to synergistic effects on grain growth and defect concentration [3]. Meanwhile,  $\text{V}_2\text{O}_5$  is a known sintering aid and can improve densification at lower temperatures, affecting dielectric relaxation behavior [4].

The sintering process plays a vital role in determining the final properties of ceramic materials. Parameters such as temperature, duration, and the number of cycles directly affect densification, porosity, grain size, and phase development. Multiple sintering cycles may lead to better

densification and improved uniformity, potentially enhancing both mechanical and electrical performance. However, excessive thermal cycling can also cause grain coarsening or undesirable phase transformations. Thus, systematically studying the effects of one, two, and three sintering cycles becomes essential to optimize the final properties of the material.[5]

This project focuses on the fabrication and characterization of doped alumina ceramics tailored for use in microwave dielectric resonators. A total of 15 samples were prepared, comprising one pure alumina pellet and four doped variants— $\text{Fe}_2\text{O}_3$ ,  $\text{Fe}_2\text{O}_3 + \text{TiO}_2$ ,  $\text{V}_2\text{O}_5$ , and  $\text{Cr}_2\text{O}_3$ —each introduced at a fixed dopant concentration of 0.1 at%. These samples were sintered under different thermal cycles (one, two, and three) to observe the effects on densification and performance.[6]

In addition, 2mm-thick polished samples of each dopant and the pure alumina were prepared for advanced analysis. These specimens were subjected to direct microwave testing, and detailed characterization techniques such as hardness testing, compression testing, Scanning Electron Microscopy (SEM), and X-Ray Diffraction (XRD) were employed to study mechanical properties, microstructural changes, and phase evolution.[7]

The overarching goal is to identify the most suitable dopant and sintering condition that enhances the dielectric and mechanical performance of alumina ceramics, thereby advancing their application in microwave resonator technology.



Fig. 1 Dielectric Resonator [1 ]

# **CHAPTER - 2**

## **LITERATURE REVIEW**

### **2.1 Dielectric Resonators**

Dielectric resonators (DRs) are non-conductive yet polarizable ceramic components designed to resonate at microwave and millimeter-wave frequencies. They confine electromagnetic energy within their volume due to the high contrast in permittivity at the boundary, leading to the formation of standing waves at specific resonant frequencies. Typically shaped as cylindrical pucks, dielectric resonators are characterized by a high dielectric constant and low dissipation factor. Their resonant frequency is a function of their physical dimensions and the dielectric constant of the material used. Initially conceptualized in the late 19th century, Lord Rayleigh[1] demonstrated that dielectric rods could guide waves, laying the groundwork for further research. By 1939, Richtmyer showed that dielectric structures could act like metal cavity resonators and coined the term “dielectric resonator.” However, the advancement of dielectric resonator technology was limited until the 1960s due to material and manufacturing constraints. The rise of high-frequency communication systems reignited interest in DRs due to their compactness, reduced weight, material availability, and cost-effectiveness compared to traditional metallic cavity resonators. In contrast to metallic cavity resonators, dielectric resonators exhibit non-zero electric and magnetic fields outside their surfaces, although these decay rapidly with distance. The energy is mostly confined within the resonator, especially for materials with a high relative permittivity ( $\epsilon_r$ ). DRs support various resonant modes, notably transverse electric (TE), transverse magnetic (TM), and hybrid electromagnetic (HEM) modes, with the  $TE_{01n}$  mode being predominant in non-radiating applications. In practical applications, DRs are usually enclosed in metallic cavities, which alters their resonant frequency due to changes in field boundary conditions. Cavity perturbation theory explains that if the displaced field energy is predominantly electric, the resonant frequency decreases; if magnetic, it increases—commonly observed in the mode. Despite their advantages, DRs are sensitive to temperature fluctuations and mechanical vibrations, which can affect frequency stability. Modern material science has mitigated some of these challenges, but compensation techniques are often necessary for precise applications. Dielectric resonators are widely utilized in filtering (bandpass and bandstop filters), oscillators (such as dielectric resonator oscillators or DROs), frequency-selective limiters, and as radiating elements in dielectric resonator antennas (DRAs). Their high Q-factor and compact form make them invaluable components in modern high-frequency electronic systems. The rapid

advancement of 5G and high-frequency telecommunication technologies has driven a parallel need for dielectric materials that offer a high dielectric constant, low dielectric loss, and thermal stability at microwave frequencies. To meet these stringent criteria, researchers have increasingly turned their attention to composite ceramics — especially those based on alumina ( $\text{Al}_2\text{O}_3$ ) and titania ( $\text{TiO}_2$ ) — due to their complementary dielectric characteristics and tunability through doping or structural modification.[1]

A pioneering step in this direction was taken by Zhenyu Tan et al.[2] who explored the influence of  $\text{TiO}_2$  addition on the microwave dielectric properties of a complex garnet-phase ceramic:  $\text{Y}_3\text{MgAl}_3\text{SiO}_{12}$ . By systematically doping this host matrix with varying concentrations of  $\text{TiO}_2$ , the authors demonstrated that not only did the densification behavior improve due to the fluxing nature of  $\text{TiO}_2$ , but the dielectric constant and quality factor ( $Q \times f$ ) also significantly increased. The microstructural refinement and enhanced polarizability arising from Ti substitution provided clear evidence that  $\text{TiO}_2$  acts as a powerful modifier for tuning microwave properties, specifically tailored for 5G communication systems. Their work confirmed that the interaction between crystal chemistry and sintering behavior could be precisely managed through controlled  $\text{TiO}_2$  incorporation.

Building on this insight, Cheng-Liang Huang and Jun-Jie Wang [3] approached the problem from a different angle by employing nano-scaled  $\alpha\text{-Al}_2\text{O}_3$  and  $\text{TiO}_2$  powders in the fabrication of sintered alumina ceramics. Their aim was to understand the synergy between particle size and composition in achieving optimal dielectric performance. The results were compelling: the use of nanostructured precursors facilitated improved grain boundary mobility and densification at lower sintering temperatures.  $\text{TiO}_2$ , in this context, not only assisted sintering but also contributed directly to dielectric behavior, enhancing the relative permittivity while maintaining low loss. These findings reinforced the idea that both composition and microstructure — particularly at the nanoscale — are pivotal to achieving the performance standards demanded by next-generation wireless technologies.

Extending the material design strategy further, T. Kolodiaznyi et al.[4] presented a comprehensive study on  $\text{Al}_2\text{O}_3\text{-TiO}_2$  composite ceramics developed specifically for millimeter-wave and high-power applications. Unlike binary mixtures, these composites leveraged intermediate phase formation, such as  $\text{Al}_2\text{TiO}_5$  deliver a stable dielectric response under thermal and electromagnetic stress. Their work highlighted that an optimal ratio between  $\text{Al}_2\text{O}_3$  and  $\text{TiO}_2$  resulted in a balance between dielectric constant, low dielectric loss, and mechanical robustness.

Importantly, the study emphasized long-term reliability and thermal cycling resistance, making their material system an ideal candidate for power-handling components in communication infrastructure. The phase evolution and structure-property relationships detailed in this work provided a holistic view of how careful engineering of Al–Ti–O systems can yield materials that meet real-world operational demands.

## **Doped Alumina Ceramics for High-Performance Microwave Resonators**

This literature review synthesizes findings from research papers focusing on the dielectric and electrical properties of various ceramic materials, with a particular emphasis on alumina and its modifications, for applications in high-performance microwave resonators and other electronic devices. The reviewed studies explore the impact of material composition, processing techniques, and doping on key properties such as dielectric constant, dielectric loss, quality factor, and electrical conductivity across different frequency and temperature ranges.

### **I. Fundamental Properties and High-Purity Alumina:**

The foundational understanding of dielectric properties is critical for microwave applications. Pure alumina ( $\alpha\text{-Al}_2\text{O}_3$ ) is a widely recognized material for high-frequency applications due to its inherent low dielectric loss. Di Marco et al. (2016) extensively investigated the dielectric properties of pure alumina from 8 GHz to 73 GHz, highlighting that achieving very low loss tangents (below  $2\times 10^{-4}$  at 8 GHz and  $5\times 10^{-4}$  at 73 GHz) is primarily dependent on the purity of the starting powders (< 50 ppm impurities) and high sintered densities (approaching theoretical density). They found that for such meticulously prepared alumina, the average grain size had a less significant impact on dielectric loss compared to impurity content and density. The consistent relative permittivity ( $\epsilon_r$ ) of 9.87 across the measured frequency range reinforces its stability for high-frequency components.[5]

### **II. Nano-Alumina and Sintering Aids:**

Improving the processing and performance of alumina, particularly through nano-scale materials and sintering aids, is a recurring theme. Huang et al. (2005) demonstrated that using nano-particle sized  $\alpha\text{-Al}_2\text{O}_3$  significantly enhances densification, enabling sintering at lower temperatures (e.g., > 99% theoretical density at 1500 °C). While the dielectric constant remained around 10, the unloaded quality factor ( $Q\times f$ ) was remarkably boosted, reaching 521,000 at 14.2 GHz for

samples sintered at 1550°C. This work established nano-alumina as a promising route for improved processability.

Building upon this, Huang and Wang (2007) further explored the effects of nano-scaled TiO<sub>2</sub> as a sintering additive to nano-scaled  $\alpha$ -Al<sub>2</sub>O<sub>3</sub>. Their research confirmed that TiO<sub>2</sub> effectively lowers the sintering temperature and dramatically enhances the Q×f values. They identified an optimal concentration of 0.5 wt% TiO<sub>2</sub> sintered at 1400°C, yielding an  $\epsilon_r$  of 9.9, a Q×f of 140,000 (at 12 GHz), and a  $\tau_f$  of -43.2 ppm/ °C. A critical finding was that the maximum Q×f occurred precisely after the eradication of the TiO<sub>2</sub> phase, indicating that the presence of free TiO<sub>2</sub> negatively affects dielectric performance.[6]

### **III. Dielectric Composites and Doping Strategies for Enhanced Functionality:**

Beyond pure or slightly modified alumina, several studies explored the integration of various dopants and composite structures to tailor electrical and dielectric properties for specific applications, including microwave absorption and energy storage.

#### **A. Transition Metal Oxides as Dopants:**

Nickel Ferrite (NiFe<sub>2</sub>O<sub>4</sub>): Paswan et al. (2022) conducted a comparative study on nanocrystalline and bulk nickel ferrite. They found that nanocrystalline NiFe<sub>2</sub>O<sub>4</sub> exhibits a higher dielectric constant compared to its bulk counterpart, attributing this to enhanced space charge polarization. Both forms displayed Maxwell-Wagner type interfacial polarization. The AC conductivity followed Jonscher's universal power law, with a transition from small polaron hopping (SPH) to correlated barrier hopping (CBH) around 200 °C. The study suggested the 700 °C sintered nanocrystalline sample's potential for high-frequency/microwave applications due to its desirable dielectric constant and low loss.

Vanadium Pentoxide (V<sub>2</sub>O<sub>5</sub>) in Mg<sub>2</sub>TiO<sub>4</sub>: Bhuyan et al. (2014) investigated V<sub>2</sub>O<sub>5</sub> as a sintering aid for Mg<sub>2</sub>TiO<sub>4</sub> (MTO) ceramics, focusing on low-temperature and broadband dielectric properties. V<sub>2</sub>O<sub>5</sub> successfully reduced the sintering temperature of MTO and improved its densification and microstructure. While it slightly increased the dielectric constant, it crucially decreased the dielectric loss, especially at cryogenic temperatures, attributed to the reduction of oxygen vacancies. This research provides valuable insights for low-temperature co-fired ceramic (LTCC) applications.[7]

**TiO<sub>2</sub> and Fe<sub>2</sub>O<sub>3</sub> in Fly Ash Ceramics:** Roy et al. (2013) explored the use of coal-fly ash, an industrial waste product, doped with TiO<sub>2</sub> and Fe<sub>2</sub>O<sub>3</sub> to produce ceramic materials with tunable electrical and dielectric properties. They observed a significant enhancement of the mullite phase, which was linked to improved electrical conductivity and dielectric constants. Both dielectric constant and loss decreased with increasing frequency, while AC conductivity increased, following Jonscher's universal power law. These doped fly ash composites showed semiconducting behavior and potential for applications in capacitors and ionic batteries.[8]

**Fe<sub>2</sub>O<sub>3</sub> in Polymer Blends:** Bafna et al. (2023) explored the dielectric parameters of Fe<sub>2</sub>O<sub>3</sub>-doped polyvinylidene fluoride (PVDF)/poly(methyl methacrylate) (PMMA) blend composites. They found that Fe<sub>2</sub>O<sub>3</sub> nanoparticles significantly increased the dielectric constant, particularly at lower frequencies, due to Maxwell-Wagner-Sillars (MWS) polarization and the formation of micro-capacitors at the interfaces. While dielectric loss increased with doping, the materials showed promise for capacitors and energy storage devices, highlighting the potential for flexible dielectric materials.[9]

**Chromium-Doped Calcium Ferrite (CaFe<sub>2</sub>O<sub>4</sub>):** UmashankaraRaja et al. (2024) synthesized chromium-doped calcium ferrite nanoparticles via a green solution combustion method. Their work showed that chromium doping maintained a single orthorhombic phase while decreasing crystallite sizes and increasing the energy band gap. Magnetic properties, specifically saturation magnetization and coercivity, were optimized at 30 mol% Cr<sup>3+</sup>. Electrically, conductivity increased linearly with frequency at lower frequencies, and the dielectric constant decreased with increasing dopant concentration. These materials show promise for memory and high-frequency devices.[10]

## **B. Composites for Microwave Absorption:**

**Al<sub>2</sub>O<sub>3</sub>-SiC Composites:** Battat and Calame (2007) investigated porous Al<sub>2</sub>O<sub>3</sub>-SiC composites for their complex dielectric permittivity behavior in the 1 MHz to 18 GHz range. They found that non-air-fired samples exhibited moderate and controllable dielectric losses, making them suitable for tunable microwave absorption. Conversely, air-fired samples showed significantly lower dielectric loss, implying that the air-firing process reduces electrical conductivity. This study highlights the importance of processing conditions in tailoring absorption properties.

**Fe/Al<sub>2</sub>O<sub>3</sub> Coatings:** Zhao et al. (2013) [11] explored Fe/Al<sub>2</sub>O<sub>3</sub> composite coatings deposited via air plasma spraying (APS) for microwave absorption. They observed that both the real ( $\epsilon'$ ) and

imaginary ( $\epsilon''$ ) parts of the complex permittivity increased significantly with higher Fe content. This was attributed to space charge polarization and the formation of an Fe conductive network, respectively. The coatings reflection loss could be varied by adjusting thickness and Fe content. Crucially, the  $\text{Al}_2\text{O}_3$  matrix allows these coatings to withstand high temperatures (beyond 600 °C), making them suitable for high-temperature microwave absorbing applications where polymer-based materials fail.

The reviewed literature collectively demonstrates the extensive research efforts in developing advanced ceramic materials for microwave applications. Pure alumina remains a benchmark for low-loss high-frequency applications, with ongoing efforts to optimize its sintering and purity. The integration of nano-sized materials and various dopants (like  $\text{TiO}_2$ ,  $\text{V}_2\text{O}_5$ ,  $\text{Fe}_2\text{O}_3$ , and  $\text{Cr}_2\text{O}_3$ ) offers versatile pathways to tailor dielectric constant, loss tangent, quality factor, and conductivity. These modifications enable improved densification at lower temperatures, enhanced performance, and the creation of specialized materials for diverse functionalities, including high-frequency resonators, capacitors, energy storage, and microwave absorption in extreme environments. The understanding of how processing parameters, material composition, and microstructure influence electrical and dielectric properties is crucial for the continued development of high-performance ceramic materials for the next generation of electronic devices.[11]

### Dopant

Dopants are added to ceramics primarily to modify their properties, such as color, electrical conductivity, or thermal stability. In this study, dopants are used exclusively for aesthetic purposes, influencing the final color of the sintered alumina-based ceramics. The selected dopants include ferric oxide ( $\text{Fe}_2\text{O}_3$ ), chromium oxide ( $\text{Cr}_2\text{O}_3$ ), vanadium oxide ( $\text{V}_2\text{O}_5$ ), and iron-titanium oxide ( $\text{Fe}_2\text{O}_3 + \text{TiO}_2$ ).

Table 1. Properties and applications of dopants [ 12 ,13,14,15].

Dopant	Density(g/cc)	Melting point(°C)	Applications
Chromium Oxide	5.21	2435	Ceramic glazes,refractories
Vanadium Pent-oxide	3.36	690	Pigments,catalysts,batteries
Ferric oxide	5.24	1565	Pigments,ferrite's,coating
Iron-Titanium Oxide	4-5	1800	coatings ,architectural ceramics

## **Role of Ferric Oxide ( $\text{Fe}_2\text{O}_3$ )**

Ferric oxide is a commonly studied dopant in ceramic systems due to its impact on grain boundary behavior and sintering dynamics. The introduction of  $\text{Fe}^{3+}$  ions into the alumina matrix helps refine the grain structure, inhibit abnormal grain growth, and promote densification during sintering. Additionally,  $\text{Fe}_2\text{O}_3$  can form secondary spinel phases (e.g.,  $\text{FeAl}_2\text{O}_4$ ) which subtly alter the dielectric constant and improve dielectric performance. Although ferric oxide does not induce strong magnetic behavior at low concentrations, it may contribute to localized polarization effects under microwave electromagnetic fields. It also serves as a sintering aid, slightly reducing sintering temperature and associated energy costs. In this study,  $\text{Fe}_2\text{O}_3$  was incorporated at a low concentration (0.1 at%) to investigate its baseline influence on the microstructure, dielectric, and mechanical properties of alumina-based ceramics.[12]

## **Co-Doping Strategy: Ferric Oxide + Titanium Dioxide ( $\text{Fe}_2\text{O}_3 + \text{TiO}_2$ )**

The combination of ferric oxide with titanium dioxide represents a co-doping strategy aimed at leveraging the synergistic effects of both dopants.  $\text{TiO}_2$ , with a high dielectric constant ( $\epsilon_r \approx 100$ ), is known to enhance the dielectric response when introduced in small amounts into ceramic matrices.  $\text{Ti}^{4+}$  ions may substitute for  $\text{Al}^{3+}$  in the alumina lattice, increasing polarizability and marginally boosting the dielectric constant. Furthermore,  $\text{TiO}_2$  contributes to grain growth control, supporting the formation of fine-grained, uniform microstructures essential for dielectric performance. When co-doped with  $\text{Fe}_2\text{O}_3$ , the system is expected to achieve improved phase stability and reduced oxygen vacancy formation, thereby minimizing dielectric losses. This co-doping route was selected to evaluate whether the combined effect of  $\text{Fe}_2\text{O}_3$  and  $\text{TiO}_2$  could outperform their individual contributions.[13]

## **Role of Vanadium Pentoxide ( $\text{V}_2\text{O}_5$ )**

Vanadium pentoxide was included in this study due to its dual role as a sintering aid and dielectric modifier.  $\text{V}_2\text{O}_5$  functions as a fluxing agent, forming transient liquid phases that enhance densification at reduced sintering temperatures. This property is valuable in reducing processing energy requirements. Additionally,  $\text{V}^{5+}$  ions can partially reduce to  $\text{V}^{4+}$  or  $\text{V}^{3+}$  states, enabling electronic transitions and dipole polarization mechanisms relevant in the microwave regime. These electronic effects may influence dielectric dispersion and tunability.  $\text{V}_2\text{O}_5$  also aids in achieving a dense microstructure with controlled porosity. Its inclusion in this work aims to explore potential improvements in dielectric loss behavior and microstructural integrity.[14]

## **Role of Chromium Oxide ( $\text{Cr}_2\text{O}_3$ )**

Chromium oxide was selected for its mechanical strengthening effect and its influence on dielectric stability.  $\text{Cr}^{3+}$  ions closely match the ionic radius of  $\text{Al}^{3+}$ , allowing substitution within the alumina lattice without causing significant lattice distortion. This substitution enhances fracture toughness and hardness, which is critical for structural reliability, especially in components subjected to mechanical stress. Additionally,  $\text{Cr}_2\text{O}_3$  maintains good dielectric performance at elevated temperatures and does not significantly increase dielectric loss, preserving the material's Q-factor. This makes it a valuable additive for achieving a balance between mechanical robustness and microwave performance.[15]

## **2.3 POST-PROCESSING**

### **2.3.1 Sintering**

Sintering is a thermal process that strengthens ceramic materials by promoting atomic diffusion and particle bonding, reducing porosity, and enhancing mechanical properties. The mechanism of sintering is driven by mass transport, where atoms move across particle boundaries, leading to densification and grain growth.

#### 1. Stages of Sintering

Sintering occurs in three main stages:

- Initial Stage:
  - Particle surfaces begin to bond, forming "necks" at contact points.
  - A small amount of densification occurs as atoms diffuse across particle interfaces.
  - Surface diffusion and grain boundary diffusion dominate this stage.
- Intermediate Stage:
  - Pores become more rounded and shrink as material continues to diffuse.
  - Neck growth increases, leading to significant densification.
  - Volume diffusion and grain boundary diffusion contribute to material transport.
- Final Stage:
  - Most of the porosity is eliminated, and grains grow significantly.
  - Small remaining pores may become trapped within grains.
  - Grain boundary sliding and coalescence occur, finalizing the microstructure.

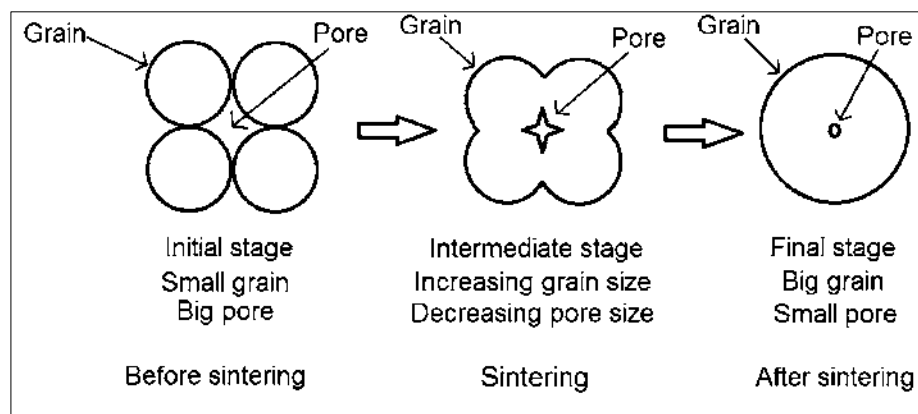


Fig.2. Stages of sintering. [9]

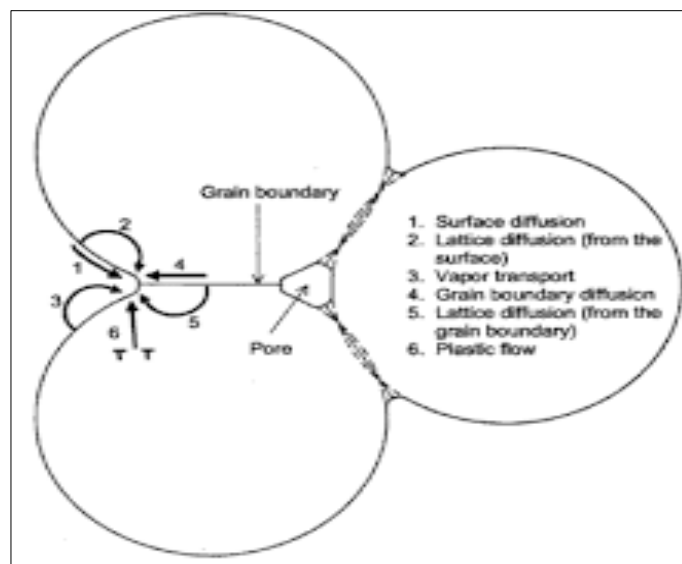


Fig.3. Sintering Mechanism. [9]

## 2. Factors Affecting Sintering

Several factors influence the sintering process and final material properties:

- Temperature: Higher temperatures increase atomic diffusion, accelerating sintering.
- Time: Longer sintering times allow more densification but can cause excessive grain growth.
- Particle Size: Smaller particles sinter faster due to increased surface area.

- Atmosphere: Controlled environments (air, vacuum, or inert gas) prevent oxidation or unwanted reactions.
- Dopants and Additives: Some elements enhance or inhibit grain growth and densification.

### 3. Sintering Outcome

Successful sintering results in a dense, mechanically strong ceramic with minimal porosity and refined grain structure. However, improper sintering can lead to warping, cracks, residual stresses, or excessive grain growth, affecting material performance.[9]

#### **2.3.2 Testing**

##### **Vector Network Analyzer (VNA)**

A Vector Network Analyzer (VNA) is a specialized electronic test instrument used to measure the network parameters of electrical networks, particularly at radio frequency (RF) and microwave frequencies. It is most commonly used to measure scattering parameters (S-parameters), which describe how RF signals behave when they encounter components such as amplifiers, filters, cables, antennas, and resonators.

The VNA is called "vector" because it can measure both the magnitude and phase of the reflected and transmitted signals. This distinguishes it from scalar network analyzers, which can only measure magnitude.

Key features of a VNA include:

- Phase and Magnitude Analysis: Allows comprehensive characterization of components, enabling accurate impedance matching and signal integrity assessment.
- Calibration Capability: Uses calibration kits to correct systematic errors and improve measurement accuracy.
- Multiple Ports: Typically configured as one-port, two-port, or multi-port depending on the complexity of the measurement.

VNA are essential in RF design, component testing, and microwave system development, where precise characterization of how signals behave through devices is critical for optimal performance. A one-port VNA setup, like the one used in this study, is particularly useful for

measuring reflection parameters such as  $S_{11}$ , which helps determine return loss, resonant frequencies, and impedance matching of the test component.[3]

## **Impedance Spectroscopy**

Impedance Spectroscopy (IS) is a powerful analytical technique used to study the electrical properties of materials and interfaces as a function of frequency. It is widely used in materials science, electrochemistry, ceramics, battery research, and sensor development.

### Principle

Impedance spectroscopy measures how a material impedes (resists and reacts to) the flow of an alternating current (AC) over a range of frequencies. It quantifies the opposition to current flow, combining:

- Resistance (R) – opposition to DC current.
- Capacitance (C) and Inductance (L) – frequency-dependent effects in AC systems.

The resulting quantity is called **impedance (Z)**, expressed as:

$$Z(\omega)=Z'+jZ''$$

### Measurement Setup

- A small AC voltage is applied across a sample.
- The resulting current is measured.
- The phase shift and amplitude change between voltage and current are analyzed to calculate impedance.

### Typical Output

#### 1. Bode Plot

The Bode plot provides frequency-dependent information in two parts: the magnitude of the impedance ( $|Z|$ ) and the phase angle ( $\theta$ ), both plotted against the logarithmic frequency scale. The magnitude plot reveals how the overall impedance of the material varies with frequency, while the phase angle plot indicates the nature of the response—resistive, capacitive, or

inductive. A flat  $|Z|$  curve generally suggests resistive behavior, whereas a downward-sloping curve indicates capacitive behavior, which is common in dielectric materials. The phase angle near  $0^\circ$  implies pure resistance, while an angle approaching  $-90^\circ$  indicates capacitive dominance. This plot is especially valuable in studying frequency-dependent dielectric behavior, identifying relaxation phenomena, and analyzing the resonance characteristics of materials used in microwave applications.[5]

## Dielectric Testing

Dielectric testing refers to a set of methods used to evaluate the electrical insulating properties of materials. These tests are crucial in determining how well a material can resist the flow of electric current, especially under high voltage or high-frequency conditions. Dielectric materials, also known as insulators, are non-conductive but polarizable, meaning they can store electrical energy when subjected to an electric field.

The primary goals of dielectric testing include:

- Determining Dielectric Constant ( $\epsilon_r$ ): This indicates how much electric energy a material can store relative to vacuum. It affects the resonant frequency in microwave components like dielectric resonators.
- Measuring Dielectric Loss (or Dissipation Factor): This evaluates how much energy is lost as heat when the material is subjected to an alternating electric field, which is vital for assessing efficiency.
- Assessing Breakdown Voltage: The maximum voltage a material can withstand without electrical failure.
- Identifying Resonant Behavior: In RF and microwave applications, dielectric testing helps identify the frequency at which the material naturally resonates when placed in a resonator configuration.

Dielectric testing becomes particularly important in high-frequency applications such as microwave filters, oscillators, and antennas, where even small losses or mismatches can impact overall system performance. Materials used in dielectric resonators, for example, are tested for high dielectric constant and low loss tangent to ensure efficient and compact designs.

Testing is typically carried out using instruments such as impedance analyzers, resonant cavity methods, or vector network analyzers (VNA), depending on the frequency range and accuracy requirements.[7]

## X-ray Diffraction (XRD)

X-ray Diffraction (XRD) is a powerful, non-destructive analytical technique used to determine the crystalline structure, phase composition, and lattice parameters of materials. It is based on the principle that X-rays, when incident on a crystalline material, are diffracted in specific directions determined by the atomic arrangement within the crystal lattice.

The technique is grounded in Bragg's Law:

$$n\lambda = 2d \sin\theta$$

where:

- n is the order of reflection,
- $\lambda$  is the X-ray wavelength,
- d is the interplanar spacing,
- $\theta$  is the angle of incidence.

Key purposes of XRD include:

1. Phase Identification: Detects and identifies different crystalline phases in a material by comparing diffraction patterns to standard reference databases.
2. Crystallinity Assessment: Determines whether a sample is crystalline, amorphous, or partially crystalline.
3. Lattice Parameter Calculation: Provides information about unit cell dimensions and strain in the crystal structure.
4. Grain Size and Texture Analysis: Can estimate crystallite size and preferred orientation of grains (texture).

XRD is widely used in materials science, metallurgy, ceramics, semiconductors, and nanotechnology for characterizing powders, thin films, and bulk solids. In the context of dielectric materials or resonators, XRD helps confirm the phase purity and crystal

structure—both of which directly influence dielectric properties such as permittivity and loss tangent.[10]

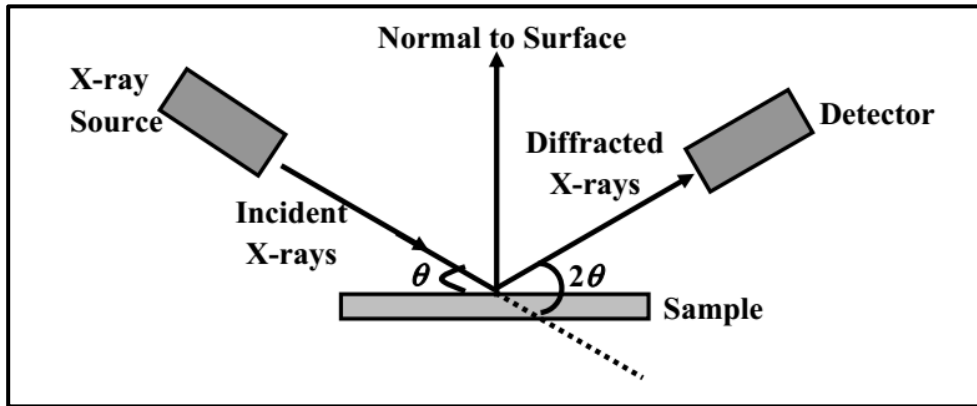


Fig.4. XRD Mechanism[10]

### 2.3.3 MECHANICAL TESTING

#### 1. Hardness testing

Hardness testing is essential for evaluating a material's resistance to localized plastic deformation, which correlates to surface durability and structural integrity. For ceramic materials such as sintered alumina and its doped variants, hardness provides a direct measure of grain bonding strength and overall densification achieved through sintering. In this project, Rockwell Superficial Hardness Testing was performed to assess the surface mechanical strength of pure and doped alumina samples fabricated under different sintering cycles. The Rockwell Superficial Hardness Test is a modified form of the standard Rockwell test, designed for thin specimens or surface-hardened materials. Unlike conventional Rockwell testing, which applies higher loads, the superficial variant uses lower minor and major loads to measure smaller penetration depths, making it ideal for materials with limited thickness or surface sensitivity—such as polished sintered pellets. The hardness value is determined by measuring the depth of the indentation made by an indentation under a minor load followed by a major load, and automatically converted into a Rockwell Superficial Hardness Number (HR). Recent advancements in Rockwell superficial hardness testing have optimized its application to ceramic systems:

- **Principle Adaptations:**

Researchers have refined this testing procedure by adjusting both the minor and major load levels to suit ceramics with high hardness yet limited thickness. For example,

adopting lower loads (3 kN minor and 15 kN major) reduces the risk of catastrophic failure while providing an accurate measure of surface hardness (Uskokovic & Riedel)

- **Measurement Accuracy:**

Several studies have demonstrated that with proper calibration and surface preparation (e.g., using MRA abrasive papers), Rockwell superficial hardness tests can yield reproducible and reliable data, making it ideal for comparing the effects of processing parameters like sintering cycles and dopant incorporation (Nakamura et al., 2017).[11]



Fig.5.Rockwell Superficial Hardness Test

## 2. Compression Test

Compression testing is a fundamental mechanical characterization technique used to evaluate a material's ability to withstand axial loads without failure. It involves applying a gradually increasing compressive force to a specimen, typically cylindrical or cuboidal in shape, until deformation or fracture occurs. This test provides critical information such as compressive strength, yield point, and modulus of elasticity. It is especially important for brittle materials like ceramics, where tensile testing is challenging due to their low ductility. Compression testing helps in understanding the load-bearing capacity and mechanical stability of materials

under service conditions, making it essential for materials selection and performance assessment in structural applications.

### Principle of Compression Testing:

Compression testing works on the principle of applying a gradually increasing axial load to a material to evaluate its strength and deformation behavior. The specimen is compressed between two platens, and its response—such as compressive strength and strain—is measured until failure or a set limit is reached.[12]

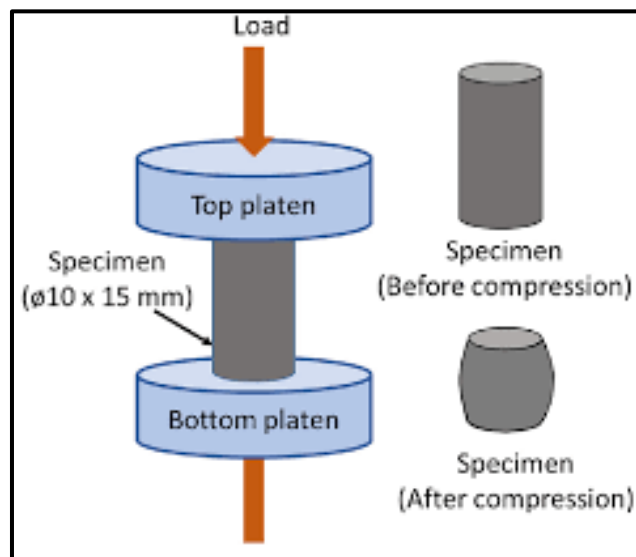


Fig 6. Compression test[12]

## CHAPTER - 3

### EXPERIMENTAL METHODOLOGY

#### **3.1 Material Selection:**

The performance of microwave dielectric resonators (MDRs) relies heavily on the material's intrinsic dielectric properties, mechanical stability, thermal resilience, and microstructural uniformity. Therefore, material selection is the most critical step in the experimental methodology as it directly affects the resonator's efficiency, signal quality, and miniaturization capability.

In this project, the base material chosen was high-purity alumina ( $\text{Al}_2\text{O}_3$ ), and four transition metal oxide dopants were selected:

1. Ferric Oxide ( $\text{Fe}_2\text{O}_3$ )
2. Titanium Dioxide ( $\text{TiO}_2$ ) combined with  $\text{Fe}_2\text{O}_3$
3. Vanadium Pentoxide ( $\text{V}_2\text{O}_5$ )
4. Chromium Oxide ( $\text{Cr}_2\text{O}_3$ )

These materials were carefully selected based on their electrical, structural, and thermal compatibility with microwave resonator applications and their potential to enhance the dielectric performance of alumina without compromising its fundamental properties.

To facilitate pellet compaction and ensure the structural integrity of green (unsintered) bodies, Polyvinyl Alcohol (PVA) was added to all formulations as a temporary organic binder.



**Fig.7. Materials Selection**

### Base Material: Alumina ( $\text{Al}_2\text{O}_3$ )

Alumina ( $\text{Al}_2\text{O}_3$ ) is one of the most widely used engineering ceramics due to its exceptional mechanical, thermal, and chemical properties. It is a high-performance oxide ceramic known for its durability, making it a preferred choice for various advanced applications. Alumina is a widely used ceramic in high-frequency electronic applications, including microwave dielectric resonators (MDRs), due to its exceptional dielectric and thermal properties. It exhibits a relatively high dielectric constant ( $\epsilon_r \approx 9-10$ ), which supports energy storage in resonator cavities and enables component miniaturization. Its low dielectric loss ( $\tan \delta < 10^{-4}$  at GHz frequencies) makes it particularly suitable for high-Q applications, where energy efficiency and signal clarity are crucial. Moreover, alumina demonstrates high thermal stability, mechanical hardness, and chemical inertness, which collectively ensure long-term performance under thermal cycling and in harsh environments.

However, despite these favorable properties, pure alumina lacks the ability to be tailored for specific dielectric requirements. This limitation has led researchers to explore doping strategies aimed at enhancing or modifying its dielectric and mechanical characteristics.

- High Mechanical Strength – Ensures structural integrity after sintering.
- Thermal Resistance – Withstands extreme temperatures up to 1600–1800°C.
- Excellent Hardness and Wear Resistance – Provides durability and long service life.
- Chemical Stability – Resistant to oxidation, corrosion, and chemical degradation.
- Electrical Insulation – Used in electronic applications due to high dielectric strength.
- Biocompatibility – Suitable for medical and dental applications.

### Applications of Alumina

Due to its outstanding properties, alumina is extensively used in:

- Aerospace: Thermal barrier coatings and high-performance components.
- Electronics: Insulators, circuit boards, and semiconductor substrates.
- Biomedical: Dental implants, hip replacements, and prosthetics.
- Automotive: Wear-resistant components and sensor housings.
- Manufacturing: Cutting tools, bearings, and wear-resistant nozzles.

### Binder: Polyvinyl Alcohol (PVA)

A binder is essential to provide extrusion stability, shape retention, and structural support before sintering. Polyvinyl alcohol (PVA) is chosen because:

- Water Solubility – Easily dissolves in water, simplifying paste preparation and removal.
- Good Film-Forming Ability – Enhances layer adhesion and surface finish.
- Biodegradability – Environmentally friendly with non-toxic properties.
- Thermal Decomposition at Low Temperatures – Reduces contamination during sintering.
- Rheological Control – Helps maintain proper viscosity and extrusion properties.

## Applications of PVA

- 3D Printing: Used in ceramic and polymer-based extrusion processes.
- Textile Industry: As a sizing agent for fabrics.
- Paper Coatings: Improves paper strength and oil resistance.
- Biomedical Applications: Used in drug delivery systems and hydrogels.

## Solvent: Distilled Water

Distilled water serves as the primary solvent to dissolve PVA and create a homogeneous ceramic paste. It is used because:

- Eliminates Impurities – Prevents contamination that could affect sintering.
- Enhances Paste Flow – Ensures proper extrusion and prevents nozzle clogging.
- Aids in Binder Activation – Helps PVA dissolve and distribute evenly in the ceramic matrix.

Table.2. Materials with its properties and applications.

Material	Density(g/cc)	Melting point(°C)	Properties	Applications
Alumina	3.95	2050(melting)	High strength,thermal resistance,hardness,electrical insulation	Aerospace,electronics,biomedical,cutting tools
Polyvinyl Alcohol(PVA)	1.19-1.31	200-350 (decomposition)	water-soluble,biodegradable,film-forming	3D printing binder, textiles
Distilled water	1	100(boiling)	Neutral pH,solvent,prevent contamination	solvent for PVA, Labs and industrial

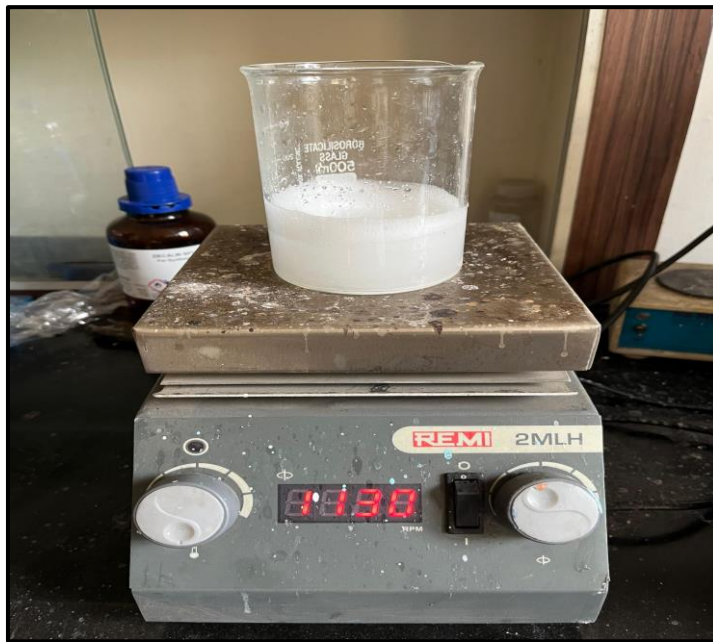


Fig.8. Binder Preparation Setup

### 3.2 Sample Preparation:

The preparation of ceramic samples is a critical stage in ensuring the reliability and repeatability of downstream testing and analysis. The sample preparation process in this study involved the precise weighing of materials, uniform mixing of dopants and binder, compaction using a hydraulic press, and controlled drying to remove volatile components. The entire procedure was carefully executed to ensure consistent dimensions, densities, and microstructures across all samples.

#### 3.2.1 Material composition

To prepare doped alumina ceramics of the general formula  $\text{Al}_{1.9}\text{M}_{0.1}\text{O}_3$  (where M = Cr, Fe, V, or a combination of Fe and Ti), precise stoichiometric calculations were carried out to determine the total molar mass and weight fractions of each component. These calculations ensure accurate doping levels and help in correlating composition with the dielectric and mechanical behavior of the sintered samples.

The total molar mass of each doped composition was computed using the following formula:

$$\text{Total molar mass} = (1.9 \times \text{Molar mass of } \text{Al}_2\text{O}_3) + (0.1 \times \text{Molar mass of dopant oxide})$$

The weight fraction of each component was then calculated as:

$$\text{Weight fraction} = \text{Molar contribution of component (g)}/\text{Total molar mass (g)}$$

The molar masses used were:

- $\text{Al}_2\text{O}_3 = 101.96 \text{ g/mol}$
- $\text{Cr}_2\text{O}_3 = 151.99 \text{ g/mol}$
- $\text{Fe}_2\text{O}_3 = 159.69 \text{ g/mol}$
- $\text{V}_2\text{O}_5 = 181.88 \text{ g/mol}$
- $\text{TiO}_2 = 79.87 \text{ g/mol}$

Table 3. Composition of each material

Composition	Total Molar Mass (g/mol)	$\text{Al}_2\text{O}_3$ (%)	Dopant(s) (%)
$\text{Al}_{1.9}\text{Cr}_{0.1}\text{O}_3$	208.923	92.74	$\text{Cr}_2\text{O}_3 = 7.26$
$\text{Al}_{1.9}\text{Fe}_{0.1}\text{O}_3$	209.693	92.48	$\text{Fe}_2\text{O}_3 = 7.62$
$\text{Al}_{1.9}\text{V}_{0.1}\text{O}_3$	211.912	91.43	$\text{V}_2\text{O}_5 = 8.58$
$\text{Al}_{1.9}\text{Fe}_{0.05}\text{Ti}_{0.05}\text{O}_3$	205.702	94.19	$\text{Fe}_2\text{O}_3 = 3.88, \text{TiO}_2 = 1.94$

### 3.2.2 Powder Weighing and Dopant Addition

The initial step in the sample preparation process involved the accurate weighing of high-purity alumina ( $\text{Al}_2\text{O}_3$ ) powder and the selected dopants. A digital analytical balance with a precision of  $\pm 0.0001 \text{ g}$  was used for this purpose. For each batch, 10 grams of alumina were weighed, and 0.1 at% of the selected dopant was added.

For the co-doped  $\text{Fe}_2\text{O}_3 + \text{TiO}_2$  samples, 0.05 at % of each oxide was used to maintain a total dopant concentration of 0.1 at %. These precise weight ratios were chosen to investigate the influence of low-concentration doping on the structural, mechanical, and dielectric properties of alumina ceramics.

### **3.2.2 Mixing and Binder Addition**

The weighted powders were then transferred to a clean, dry mortar and pestle for manual mixing. This approach allowed for controlled and thorough blending of the base alumina with the dopant, ensuring uniform distribution of the additive throughout the matrix.

To enhance the binding between particles and improve the green strength of the compacted samples, a small amount of Polyvinyl Alcohol (PVA) solution was added during mixing. The PVA binder, known for its excellent water solubility and clean thermal decomposition, was added dropwise while mixing until a slightly moist, granular consistency was achieved. This binder played a crucial role in maintaining the structural integrity of the green pellets prior to sintering.



Fig. 9 Mortar Pestle (Mixing)

### **3.2.3 Pellet Formation Using Hydraulic Press**

The uniformly mixed powder was then loaded into a 14 mm diameter steel die, which was lubricated with stearic acid and acetone to prevent sticking and ensure smooth ejection of the formed pellet. Each pellet was compacted using a hydraulic press at a pressure of 2 tons (approximately 2000 kg-force), applied uniformly for several seconds.

This process was repeated to create a total of 15 larger pellets, divided as follows:

- 3 pure alumina samples (control group)
- 3 samples each for the four doped groups: Fe<sub>2</sub>O<sub>3</sub>, Fe<sub>2</sub>O<sub>3</sub> + TiO<sub>2</sub>, V<sub>2</sub>O<sub>5</sub>, and Cr<sub>2</sub>O<sub>3</sub>

Additionally, 10 smaller cylindrical samples, each with approximately 14 mm diameter and around 2-3 mm thickness, were fabricated using a smaller mold and the same material formulations. These smaller specimens were specifically intended for XRD, and microwave testing, where minimal sample size is preferred for ease of analysis and equipment compatibility.



Fig.10. Hydraulic Press



Fig.11.Pellets

### **3.2.4 Drying and Debinding**

Following pelletization, the green samples were placed in a hot air oven and dried at 120°C for 2–3 hours. This step served two purposes:

1. Evaporation of residual moisture introduced during binder addition.
2. Thermal decomposition and removal of PVA binder (debinding) to prevent defects such as cracking or bloating during the subsequent high-temperature sintering stage. This controlled drying process ensured that the samples maintained their mechanical integrity and dimensional accuracy before entering the sintering stage.



Fig.12. Hot Oven Drying

### **3.3 Sintering Procedure:**

All sintering operations were carried out using a programmable high-temperature muffle furnace, capable of achieving temperatures up to 1600°C with precise control over heating rate, dwell time, and cooling profiles.

The 15 large pellets (14 mm diameter) were divided into three distinct groups, each consisting of five samples:

- Batch 1: Subjected to one sintering cycle
- Batch 2: Subjected to two complete sintering cycles
- Batch 3: Subjected to three complete sintering cycles

This experimental design allowed us to study the effect of sintering frequency on densification, grain structure, and dielectric behavior.

Additionally, all ten smaller samples (14 mm × 2-3 mm), prepared for advanced characterization (XRD, microwave testing), were subjected to all three sintering cycles to ensure uniform thermal conditioning and maximize structural refinement.

#### Thermal Profile and Cycle Parameters:

##### Step 1: Initial Heating

- Ramp rate: 5°C/min
- Target temperature: 500°C
- Holding time: 30 minutes
- Purpose: Controlled decomposition of residual organics (mainly PVA binder) and removal of absorbed moisture.

##### Step 2: Intermediate Soak

- Ramp rate: 7°C/min
- Target temperature: 1000°C
- Holding time: 15 minutes
- Purpose: Initiates solid-state diffusion and early-stage neck formation between particles.

##### Step 3: Final Sintering Soak

- Ramp rate: 7°C/min
- Target temperature: 1475°C
- Holding time: 4 hours
- Purpose: Achieves full densification, promotes grain growth, and enables dopant incorporation or secondary phase development.

#### Cooling

- Method: Furnace cooling (natural cooling with the furnace turned off)
- Purpose: Prevents thermal shock and cracks by allowing gradual cooling; supports uniform grain boundary relaxation.

This sintering schedule was designed to balance densification and grain growth control, ensuring sufficient diffusion without causing exaggerated grain coarsening or pore trapping.



Fig. 13. Muffle Furnace



Fig.14. Pellets after Sintering

### 3.4 Surface Preparation (Polishing)

Polishing is a crucial post-sintering step in ceramic processing, especially when the samples are to be subjected to surface-sensitive tests such as mechanical hardness measurements and

dielectric property evaluation. Surface irregularities, residual porosity, and micro-cracks can significantly influence test results and introduce inconsistencies. Therefore, achieving a smooth, uniform surface is essential for ensuring reliable and repeatable measurements.

### 3.4.1 Polishing of Main Samples (14 mm Pellets)

After sintering, all 15 large samples (14 mm in diameter) were subjected to manual polishing using MRA abrasive papers. The polishing process was conducted in a progressive sequence from coarse to finer grit sizes to gradually eliminate surface roughness and obtain a flat, reflective surface.

- The procedure began with medium-grit MRA paper (e.g., 400 grit) to remove any surface glazing, warping, or sintering-induced residues.
- It was followed by finer grits (e.g., 800 and 1200 grit) to refine the surface and remove scratches left from earlier stages.

This preparation was essential for mechanical tests (e.g., hardness, compression) and dielectric measurements, where surface uniformity influences indentation accuracy and dielectric field interactions.

### 3.4.2 Polishing and Division of 2 mm Samples

The smaller 2 mm cylindrical samples (fabricated from each composition) were specifically prepared for advanced characterization. These were divided into two equal groups:

- Group A (5 samples): Polished using the same MRA paper sequence as the larger samples. These samples were intended for:
  - Direct dielectric testing, where surface smoothness helps ensure stable contact and field uniformity during RF signal excitation.
- Group B (5 samples): Left unpolished and were directly used for X-Ray Diffraction (XRD) analysis. Polishing was intentionally avoided in this case to preserve the original surface crystallography and prevent distortion or smearing of surface lattice planes, which could interfere with accurate phase identification during XRD scans. XRD requires relatively untouched surfaces to capture precise diffraction patterns from crystallographic planes.

### **3.5 Dielectric Characterization Using Vector Network Analyzer (VNA)**

To evaluate the microwave performance of alumina-based ceramic materials, dielectric characterization was performed using a Vector Network Analyzer (VNA). The key parameters assessed were the real part of permittivity ( $\epsilon'$ ), indicating energy storage, and the imaginary part ( $\epsilon''$ ), related to energy loss.

#### 3.5.1 Equipment and Setup

Measurements were conducted using a VNA connected to a coaxial probe. Five dense, polished ceramic samples were selected based on their surface finish and structural integrity. The probe setup ensured minimal air gaps and consistent contact during testing.

#### 3.5.2 Procedure

1. **Calibration:** The system was calibrated using water to eliminate probe reflection effects.
2. **Sample Contact:** Polished samples were placed under the probe at room temperature with gentle contact.
3. **Frequency Sweep:** The VNA swept across the 3–10 GHz range, recording  $\epsilon'$ ,  $\epsilon''$ , and  $\tan \delta$  values in real time.

#### 3.5.3 Data Analysis

- **Dielectric Constant ( $\epsilon'$ ):** Reflects energy storage, important for miniaturization.
- **Dielectric Loss ( $\epsilon''$ ):** Indicates internal energy dissipation.
- **Loss Tangent ( $\tan \delta = \epsilon'' / \epsilon'$ ):** Key for high-Q resonators; lower values ( $< 10^{-3}$ ) indicate better performance.

This method provided accurate, non-destructive characterization of the ceramic materials, supporting their suitability for microwave dielectric resonator applications.

VNA measurements were conducted using the Keysight Technologies N5222B (SN: MY51421600, Firmware: A.17.35.14) via the Coaxial Probe Method (v16.0.16092801). A high-temperature coaxial probe was used with calibration standards of air, short, and 25°C water. The measurement was performed on Channel 1, Port 1, with an IF bandwidth of 300 Hz and input power of 0 dBm.

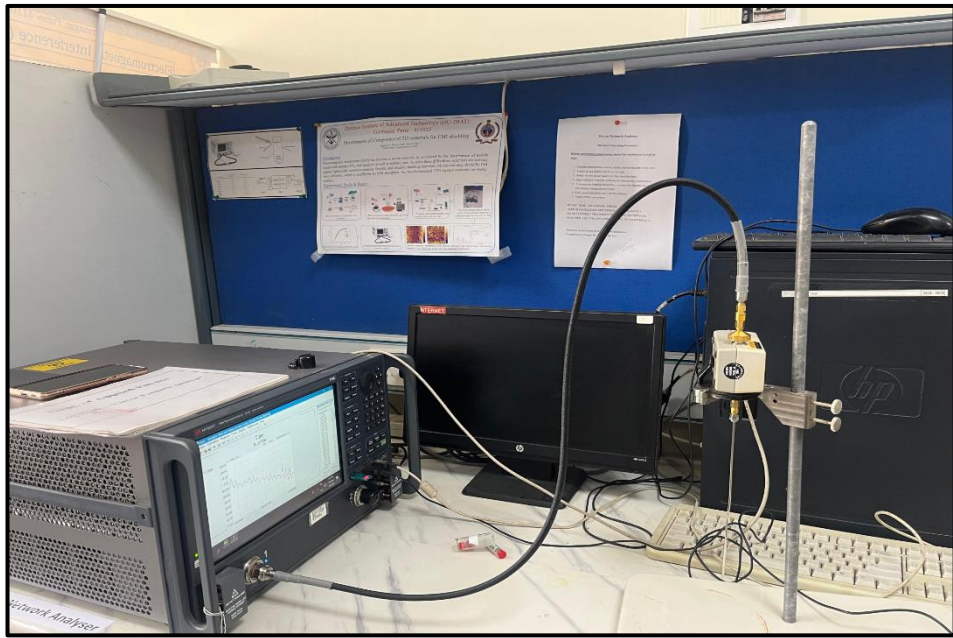


Fig.15. VNA Experimental Setup

### 3.6 Impedance Spectroscopy

Dielectric testing is essential for evaluating a material's ability to store and transmit electromagnetic energy, particularly in microwave dielectric resonator (MDR) applications. In this study, impedance spectroscopy was used to assess the dielectric performance of polished alumina samples—pure and doped with  $\text{Fe}_2\text{O}_3$ ,  $\text{Fe}_2\text{O}_3 + \text{TiO}_2$ ,  $\text{V}_2\text{O}_5$ , and  $\text{Cr}_2\text{O}_3$ .

Five cylindrical samples (14 mm diameter, 2 mm thick), each subjected to triple sintering for improved density and crystallinity, were selected. Their surfaces were finely polished to ensure reliable probe contact and minimize measurement error.

#### 3.6.1 Testing Setup and Procedure

- Dielectric measurements were performed using a calibrated microwave testing system, likely based on the cavity resonator or coaxial probe method. Calibration (e.g., open-short-load) was first conducted to eliminate system errors. Each sample was carefully loaded into a holder with firm, gap-free contact.
- During testing, microwave signals were transmitted, and parameters such as resonant frequency, return loss, and Q-factor were measured. Data was recorded and analyzed through connected software.



Fig.16. Dielectric Testing Experimental setup

### 3.7 Mechanical Testing

#### 3.7.1 Rockwell Superficial Hardness Testing

##### Equipment and Setup

- Instrument: Rockwell Superficial Hardness Tester
- Indenter: Steel ball or diamond cone (Brake), depending on the superficial scale used
- Minor Load: Approximately 3 kN (3000 N)
- Major Load: Approximately 15 kN (15000 N)
  
- Sample Type: 14 mm diameter × 3–5 mm thick sintered pellets
- Surface Condition: All samples were polished using MRA abrasive papers prior to testing

##### Testing Procedure

###### 1. **Sample Preparation:**

- All samples were pre-polished to achieve a flat and smooth surface, reducing surface irregularities that could affect the indentation depth or contact area.

## **2. Sample Positioning:**

- Each sample was carefully placed on the anvil of the tester, centered beneath the indenter to ensure vertical loading and prevent edge effects.

## **3. Load Application:**

- A minor load of 3 kN was first applied to seat the indenter into the surface.
- This was followed by the major load of 15 kN, which was held momentarily during the test cycle.
- The difference in indentation depth before and after the application of the major load was measured to calculate the hardness.

## **4. Dwell Time Clarification:**

- While Rockwell hardness tests typically use a dwell time of 10–15 seconds, the reference to 30 minutes is interpreted as the total operational duration per sample, including sample placement, stabilization, and repeated trials—not the indenter's contact time.

## **5. Repetition and Averaging:**

- The hardness test was repeated three times per sample at different surface locations to account for potential material inhomogeneity.
- The average of the three readings was calculated and recorded as the final hardness value for each sample.



Fig.17. Rockwell Superficial Hardness Tester

### **3.7.2 Compression Testing:**

Calibration:

- The Universal Testing Machine (UTM) was calibrated before initiating the tests to ensure precision and accuracy in the results.
- Calibration was done according to standard protocol to minimize machine error and maintain consistency across all measurements.

Sample Placement:

- Cylindrical samples were carefully positioned on the lower platen of the UTM.
- Care was taken to ensure the flat surface of the specimen was in full contact with the platen to avoid any tilting or instability.

Alignment:

- The upper compression platen was adjusted to be perfectly aligned with the axis of the specimen.
- Proper axial alignment was ensured to avoid eccentric loading, which can affect fracture behavior and recorded strength.

Compression Test Execution:

- The UTM was set to compression mode with a constant crosshead speed.
- Load was applied gradually to the specimen until either fracture occurred or the maximum load was achieved.
- The machine automatically stopped recording once the sample failed or showed a significant drop in the stress-strain curve.

Data Recording:

- During the test, both force (in Newtons) and displacement (in millimeters) were recorded in real time using the UTM software.

Repetition:

- Each test was repeated for five samples of each type (pure alumina, Cr<sub>2</sub>O<sub>3</sub> doped, V<sub>2</sub>O<sub>5</sub> doped, Fe<sub>2</sub>O<sub>3</sub> doped, and Fe<sub>2</sub>O<sub>3</sub> + TiO<sub>2</sub> doped).
- This was done for three different sintering cycles – once sintered, twice sintered, and thrice sintered – resulting in 15 samples in total.
- Repeating the tests ensured statistical accuracy and helped identify any variation due to sample inconsistencies.

Post-Test Handling:

- After testing, broken samples were carefully removed and disposed of following lab safety guidelines.
- The platens were cleaned before testing the next sample to maintain surface condition.



Fig.18. Compression Testing (UTM Machine)

### **3.8 XRD:**

X-Ray Diffraction (XRD) is a non-destructive analytical technique used to determine the crystallographic structure, phase composition, and dopant-induced lattice changes in polycrystalline materials. In the context of this project, XRD was employed to investigate the effect of low-level doping and multi-cycle sintering on the phase stability and structural evolution of alumina ceramics.

#### Sample Selection and Preparation

A total of five unpolished samples were selected for XRD analysis—each representing one of the following compositions:

- Pure Alumina (control)

- Alumina + Fe<sub>2</sub>O<sub>3</sub>
- Alumina + Fe<sub>2</sub>O<sub>3</sub> + TiO<sub>2</sub>
- Alumina + V<sub>2</sub>O<sub>5</sub>
- Alumina + Cr<sub>2</sub>O<sub>3</sub>

All samples were 14 mm in diameter and around 2-3 mm thick, prepared as described in the sintering stage and left unpolished specifically to avoid surface modification that could affect XRD patterns. The unaltered surface preserves the integrity of the surface lattice planes and ensures accurate detection of diffraction peaks.



Fig. 19. XRD

# CHAPTER - 4

## RESULT AND DISCUSSION

### 4.1 Density Measurement

The density values of cylindrical ceramic samples were calculated using their respective mass, diameter, and height measurements. The results revealed noticeable variation in density among different samples, primarily influenced by factors such as material composition, compaction quality, and sintering behavior.

Higher density values typically suggest better particle packing, lower porosity, and more effective sintering. Conversely, lower densities may indicate the presence of internal voids, poor compaction, or insufficient densification during sintering. These differences in density are crucial as they directly impact the mechanical and functional properties of the final material.

Table 4. Density measurement

Dopant	Diameter of pellet(mm)	Density as per rule of mixture	Density(g/cc)
Pure Alumina	12.73	3.95	3.11
Cr <sub>2</sub> O <sub>3</sub> doped	13.09	4.02	2.99
V <sub>2</sub> O <sub>5</sub> doped	13.16	3.89	3.02
Fe <sub>2</sub> O <sub>3</sub> doped	12.41	4.02	3.12
Fe <sub>2</sub> O <sub>3</sub> +TiO <sub>2</sub> doped	12.28	3.99	3.45

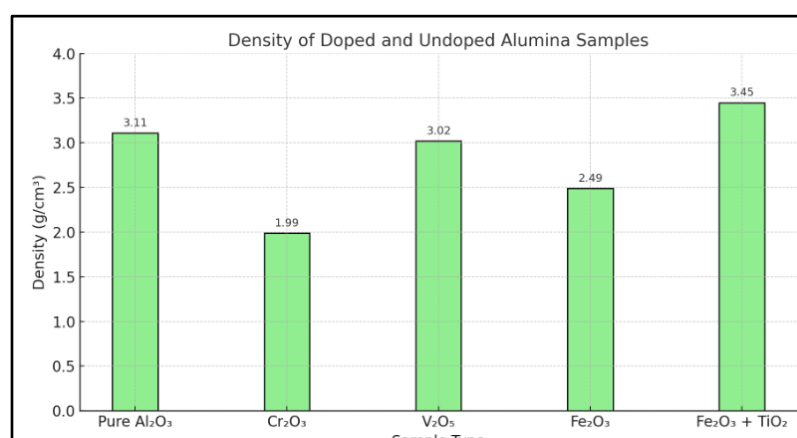


Fig 20. Density of doped and undoped alumina samples

## 4.2 XRD

The X-ray diffraction (XRD) analysis of pure and doped alumina samples provides valuable insights into the structural stability and phase composition of the materials. Across all the examined specimens—pure alumina, Cr<sub>2</sub>O<sub>3</sub>-doped, V<sub>2</sub>O<sub>5</sub>-doped, Fe<sub>2</sub>O<sub>3</sub>-doped, and Fe<sub>2</sub>O<sub>3</sub> + TiO<sub>2</sub>-doped—the XRD patterns predominantly show a single-phase structure. This indicates that the incorporation of dopants in small quantities did not result in the formation of any distinct new crystalline phases or significant structural changes in the host matrix. The positions and intensities of the peaks in the doped samples largely match those of the undoped alumina, suggesting that the dopant atoms have either substituted within the alumina lattice or remained in solid solution without disrupting the overall crystallographic order.

The retention of this single-phase nature even after doping implies that the selected doping concentrations were within the solubility limits of alumina. This structural consistency is particularly important, as it demonstrates that the dopants did not segregate into separate phases during the sintering process, which could otherwise negatively impact the material's uniformity and performance. The peak shapes and positions remained sharp and consistent, further confirming the crystalline integrity of the samples.

An exception was observed in the Fe<sub>2</sub>O<sub>3</sub> + TiO<sub>2</sub> doped sample, where additional minor peaks were detected in the XRD spectrum. These new peaks suggest the possible formation of small amounts of secondary phase(s), potentially due to interactions between the iron and titanium oxides at elevated temperatures. Despite this, the dominant phase remains similar to that of undoped alumina, and the structural framework is not significantly altered.

In conclusion, the XRD results confirm that doping with Cr<sub>2</sub>O<sub>3</sub>, V<sub>2</sub>O<sub>5</sub>, and Fe<sub>2</sub>O<sub>3</sub> in low concentrations does not lead to any noticeable changes in phase composition, preserving the structural characteristics of alumina. Only in the case of Fe<sub>2</sub>O<sub>3</sub> + TiO<sub>2</sub>, slight evidence of secondary phase formation is visible, which could be attributed to chemical reactions between the two dopants during sintering.

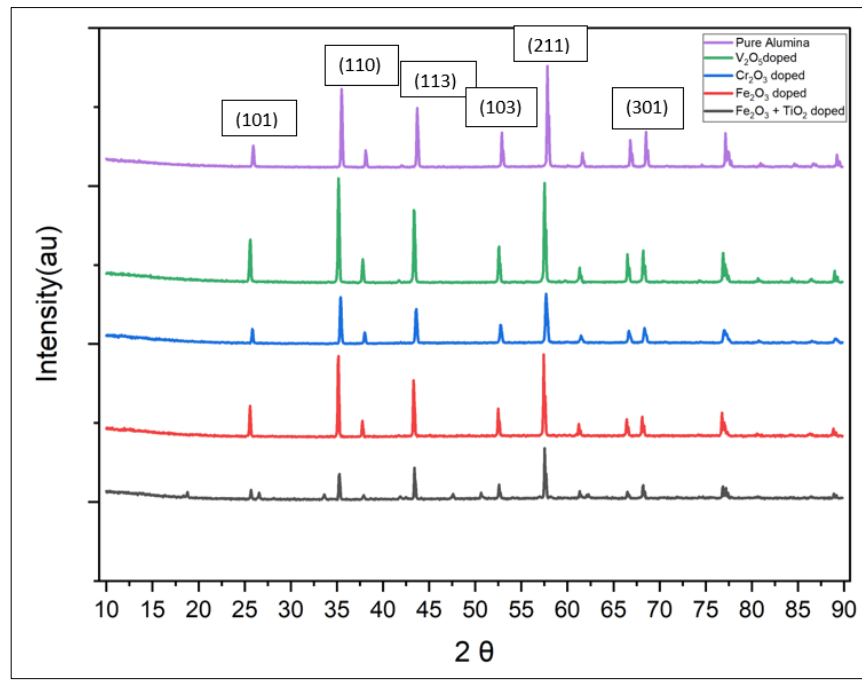


Fig.21. XRD Analysis(JCPDS: 00-046-1212)

## 4.2 Dielectric Properties

### 4.2.1 Bode plot

The graph illustrates the frequency-dependent behavior of the real part of impedance ( $Z'$ ) for pure and doped alumina ceramic samples, including 0.1 at% dopants such as  $Cr_2O_3$ ,  $Fe_2O_3$ ,  $V_2O_5$ , and a combination of  $Fe_2O_3+TiO_2$ . While  $Al_2O_3$  is purely a insulator, doping of transition metal oxides has introduced marginal semiconductor behaviour. All samples exhibit a common trend where  $Z'$  decreases with increasing frequency, a characteristic feature of semiconducting materials. This decline is more prominent at lower frequencies due to the dominance of space charge polarization and interfacial effects. Among the samples, Fe-doped alumina demonstrates the highest  $Z'$  values, suggesting it has the greatest resistance to charge transport. This behavior indicates significant charge carrier obstruction and may be attributed to localized states induced by Fe ions.

As the frequency increases, the impedance values for all samples begin to converge. This merging of  $Z'$  curves at higher frequencies is associated with a reduction in polarization effects and space charge relaxation, leading to a more intrinsic response of the bulk material. Such behavior is indicative of negative temperature coefficient of resistance (NTCR), where resistivity decreases with increasing temperature or frequency. The Cr- and V-doped samples show comparatively lower  $Z'$  values across the frequency range, which points to improved AC

conductivity and enhanced electrical transport properties in those compositions.

These results align well with literature reports on spinel ferrites and other ceramic systems, where doping plays a crucial role in tuning the electrical properties. The enhanced impedance in Fe-doped samples may be due to defect states or barriers introduced at the grain boundaries. This rise helps to reduce signal losses, improve signal integrity and enhance performances of electrical component, noise reduction and reduced power consumption, while reduced impedance in Cr- and V-doped samples may result from enhanced hopping conduction or lower barrier heights. Overall, the study confirms that selective doping in alumina ceramics can significantly influence the impedance behavior, supporting their potential application in high-frequency dielectric and electronic devices.

Table 5. Value of Z' w.r.t Frequency(Hz)

Frequency (Hz)	Pure Al <sub>2</sub> O <sub>3</sub> ( $\Omega$ )	Cr <sub>2</sub> O <sub>3</sub> ( $\Omega$ )	Fe <sub>2</sub> O <sub>3</sub> ( $\Omega$ )	Fe <sub>2</sub> O <sub>3</sub> + TiO <sub>2</sub> ( $\Omega$ )	V <sub>2</sub> O <sub>5</sub> ( $\Omega$ )
10 <sup>0</sup> (1 Hz)	3.10E+07	2.12E+07	3.16E+08	4.82E+07	1.88E+07
10 <sup>1</sup> (10 Hz)	2.57E+07	1.96E+07	2.23E+08	4.38E+07	1.82E+07
10 <sup>2</sup> (100 Hz)	1.85E+07	1.52E+07	1.22E+08	3.35E+07	1.65E+07
10 <sup>3</sup> (1 kHz)	1.01E+07	8.04E+06	2.73E+07	1.63E+07	1.06E+07
10 <sup>4</sup> (10 kHz)	4.47E+06	3.83E+06	1.14E+07	7.88E+06	3.55E+06
10 <sup>5</sup> (100 kHz)	2.83E+06	2.70E+06	1.29E+07	5.97E+06	3.16E+06

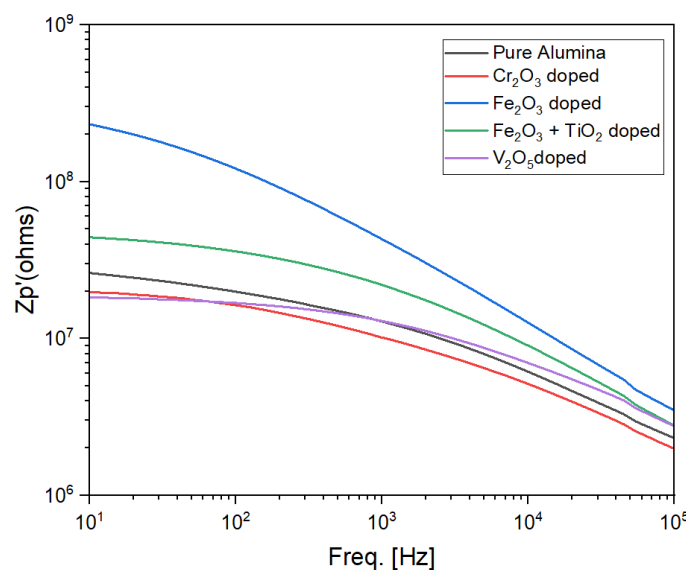


Fig. 23. Bode Plot

#### **4.2.2 Dielectric constant-Impedance Spectroscopy**

The plot of the dielectric constant ( $\epsilon'$ ) versus frequency for pure alumina and various doped alumina ceramics ( $\text{Cr}_2\text{O}_3$ ,  $\text{Fe}_2\text{O}_3$ ,  $\text{Fe}_2\text{O}_3 + \text{TiO}_2$ , and  $\text{V}_2\text{O}_5$ ) displays a typical dispersive behavior common in ceramic materials. Initially, the dielectric constant is high at lower frequencies and decreases significantly as the frequency increases. This behavior can be attributed to the contributions of multiple polarization mechanisms. At low frequencies, interfacial or space charge polarization dominates. This is well explained by Koop's theory and the Maxwell-Wagner (M-W) model, which suggest that ceramic materials consist of highly conductive grains separated by resistive grain boundaries. At these low frequencies, charge carriers accumulate at the grain boundaries, resulting in enhanced polarization and thus a higher dielectric constant.

In addition to interfacial polarization, other polarization mechanisms also play a role. Dipolar polarization occurs due to the alignment of permanent or induced dipoles in the material under the influence of an electric field. This mechanism is prominent at low to moderate frequencies. Ionic polarization results from the relative displacement of positive and negative ions in the lattice structure when an electric field is applied, and electronic polarization arises from the displacement of electron clouds relative to their nuclei. As frequency increases, these slower polarization mechanisms can no longer keep up with the rapidly oscillating electric field, leading to a reduction in the dielectric constant.

The graph shows that pure alumina has the highest dielectric constant at low frequency, but as frequency increases (particularly near  $10^3$  Hz), it drops to approximately 8.05. Among the doped samples, Cr-doped alumina exhibits the highest dielectric constant at  $10^3$  Hz (around 8.47), while  $\text{V}_2\text{O}_5$ -doped alumina shows the lowest value (approximately 6.3). The difference in dielectric constants at this frequency is relatively small (around 2.2 units), indicating that doping has a moderate but distinguishable effect on dielectric behavior. These differences may be due to localized charge hopping processes such as  $\text{Fe}^{3+}/\text{Fe}^{2+}$  or  $\text{Cr}^{3+}/\text{Cr}^{2+}$  redox pairs, which enhance polarization at low frequencies.

The observed rise and subsequent fall of  $\epsilon'$  across the frequency range is a strong indicator of frequency-dependent polarization mechanisms. At low frequencies, enhanced polarization due to charge accumulation at grain boundaries and possible redox activity increases  $\epsilon'$ , while at high frequencies, the lag in polarization response leads to its decline. This comprehensive behavior is characteristic of ceramic dielectrics and supports the proposed theories of polarization in such materials.

Table 6. Dielectric constant value at  $10^3$  Hz

Dopant added(0.2 wt%)	Dielectric Constant at $10^3$ Hz
Pure Alumina	8.06
$\text{Cr}_2\text{O}_3$ doped	8.5
$\text{V}_2\text{O}_5$ doped	6.2
$\text{Fe}_2\text{O}_3$ doped	6.3
$\text{Fe}_2\text{O}_3 + \text{TiO}_2$ doped	7.2

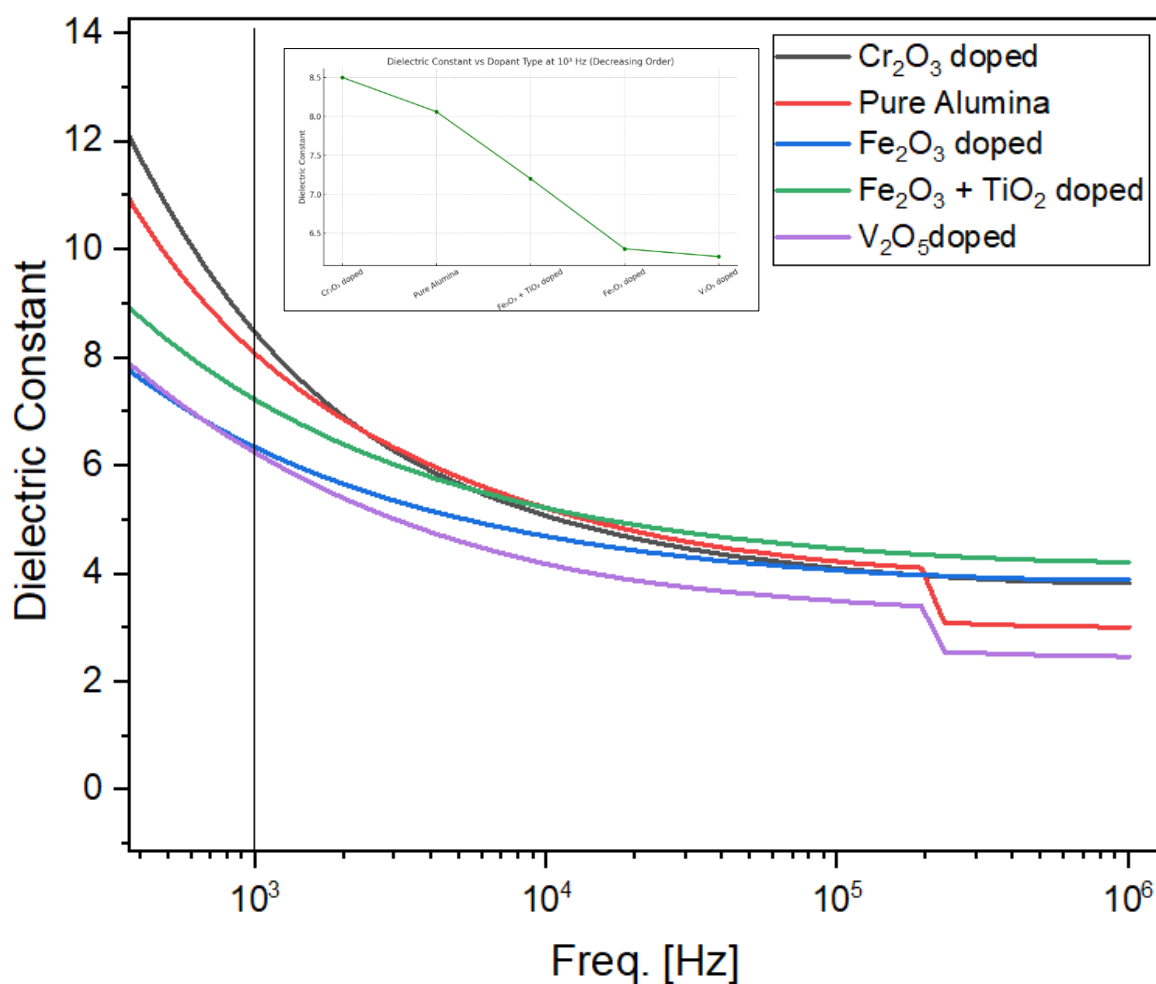


Fig. 24. Dielectric Constant Vs Frequency [Hz]

### 4.2.3 Dielectric Loss-Impedance Spectroscopy

The dielectric loss ( $\tan \delta$ ) versus frequency graph for pure and doped alumina samples reveals a clear decreasing trend in dielectric loss with increasing frequency across all compositions. At low frequencies (around  $10^2$  Hz), the dielectric loss is highest for the  $V_2O_5$  doped sample (6.0), followed by pure alumina (3.5),  $Cr_2O_3$ -doped (2.5),  $Fe_2O_3 + TiO_2$  doped (2.0), and is lowest for  $Fe_2O_3$  doped alumina (0.8). As the frequency increases to the mid-range ( $10^3$ – $10^5$  Hz), all samples exhibit a steady decline in  $\tan \delta$  due to the inability of hopping charge carriers and dipolar species to keep pace with the rapidly oscillating electric field. At high frequencies (above  $10^5$  Hz), the dielectric loss values converge and become nearly constant and very low (in the range of 0.005 to 0.01), indicating minimal energy dissipation. This behavior corresponds well with the literature, which attributes high dielectric loss at low frequencies to interfacial (Maxwell–Wagner) polarization, grain boundary resistance, and charge carrier hopping, especially in transition metal-doped ceramics.

Table 7. Tangent loss value of sample w.r.t Frequency(Hz)

Dopant Added (0.2 wt%)	$\tan \delta$ at $10^2$ Hz	$\tan \delta$ at $10^3$ Hz	$\tan \delta$ at $10^5$ Hz
Pure Alumina	3.5	1.2	0.005
$Cr_2O_3$ Doped	2.5	1.0	0.005
$V_2O_5$ Doped	6.0	2.5	0.010
$Fe_2O_3$ Doped	0.8	0.5	0.005
$Fe_2O_3 + TiO_2$ Doped	2.0	0.8	0.005

As the frequency increases, these mechanisms cannot follow the field, leading to reduced losses. The effect of doping is significant:  $Fe_2O_3$ -doped alumina exhibits the lowest dielectric loss across the spectrum, likely due to reduced defect concentrations and improved microstructural uniformity. The  $Fe_2O_3 + TiO_2$  co-doped sample also maintains low  $\tan \delta$ , while  $Cr_2O_3$  provides moderate improvement over pure alumina. Conversely,  $V_2O_5$  doping leads to the highest dielectric loss, suggesting that it introduces oxygen vacancies and weakens grain boundary resistivity, thereby enhancing charge hopping and energy dissipation. Overall, low dielectric loss, particularly in the  $Fe_2O_3$  and  $Fe_2O_3 + TiO_2$  doped samples, suggests their suitability for high-frequency and microwave applications where dielectric stability and low energy dissipation

are crucial. This graph supports the theoretical understanding of dielectric behavior in doped ceramics and highlights the role of dopants in tailoring the electrical performance of alumina-based materials.

Table 8. Effect of each dopant on tangent loss

Dopant	Effect on $\tan \delta$	Explanation
$\text{Fe}_2\text{O}_3$	Lowest loss	Fills oxygen vacancies, reduces defect-related hopping.
$\text{Fe}_2\text{O}_3 + \text{TiO}_2$	Slightly more than $\text{Fe}_2\text{O}_3$	$\text{Ti}^{4+}$ may introduce new relaxation sites but still low loss.
$\text{Cr}_2\text{O}_3$	Moderate loss	Improves density, but residual porosity may cause mild hopping.
Pure	Higher than Cr	No dopant to control oxygen vacancies or enhance microstructure.
$\text{V}_2\text{O}_5$	Highest loss	Introduces oxygen vacancies, weakens grain boundary resistance.

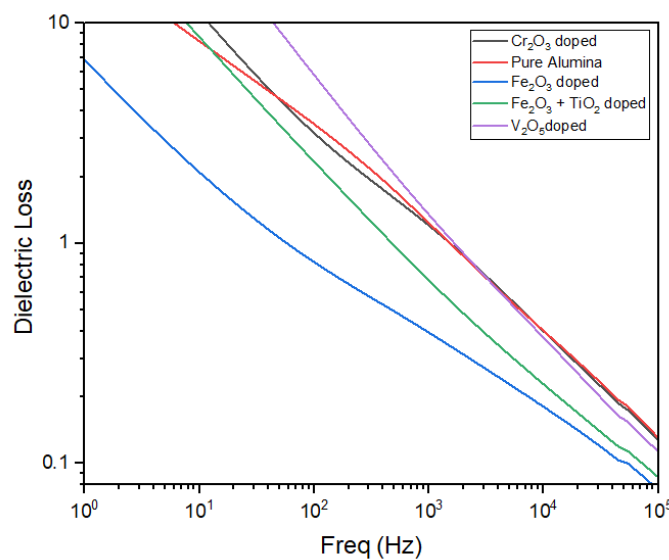


Fig.25. Dielectric Loss Vs Frequency [Hz]

#### **4.2.4 Dielectric constant- VNA**

The dielectric behavior of doped alumina ceramics was comprehensively analyzed using a Vector Network Analyzer (VNA), focusing on how the dielectric constant varies with frequency for samples doped with  $\text{FeTiO}_2$  and Cr oxides. These dopants were chosen due to their known influence on ceramic microstructure and electrical properties. The frequency-dependent dielectric constant provides insight into the polarization mechanisms active in the material, especially at microwave frequencies relevant for dielectric resonators and communication devices.

From the VNA data presented in the graph ,it is evident that the  $\text{FeTiO}_2$ -doped alumina sample consistently shows a higher dielectric constant (DC) across the frequency range compared to the Cr-doped counterpart. This downward trend with increasing frequency is expected, as dielectric polarization mechanisms—especially dipolar and space charge polarization—tend to lag behind the rapidly oscillating electric fields at higher frequencies.

The superior dielectric constant in  $\text{FeTiO}_2$ -doped samples can be attributed to the synergistic effects of iron and titanium ions.  $\text{Fe}^{3+}$  and  $\text{Ti}^{4+}$  have different ionic radii and valances compared to  $\text{Al}^{3+}$  in the alumina lattice, which likely introduces localized distortion and increased lattice defects. These imperfections can enhance space charge polarization, especially at grain boundaries, thereby increasing the dielectric constant. The combined effect of these dopants may also influence the electronic polarizability due to the higher polarizing power of Fe and Ti compared to Cr (Liu et al., 2018)[5]. Moreover,  $\text{FeTiO}_2$  doping might enhance the overall density and connectivity of grains, contributing to better dielectric properties.

To further interpret these results from a microstructural perspective, XRD-based FWHM (Full Width at Half Maximum) data were analyzed, as shown in the graph . FWHM is inversely related to crystallite size and directly associated with internal lattice strain. The  $\text{FeTiO}_2$ -doped samples exhibit FWHM values which are notably broader than those observed for the Cr-doped samples. According to Cullity and Stock (2001)[6], broader peaks reflect smaller crystallite sizes and/or higher microstrain. These microstructural features promote enhanced interfacial polarization by increasing grain boundary density and active charge accumulation sites, thereby contributing to the higher dielectric constant observed in  $\text{Fe}_2\text{O}_3+\text{TiO}_2$ -doped alumina.

Additionally,  $\text{Fe}_2\text{O}_3+\text{TiO}_2$  doping likely creates a more refined and strained microstructure compared to Cr doping.  $\text{Cr}^{3+}$  ions substitute more symmetrically into the alumina lattice and may

not contribute as significantly to interfacial polarization as  $\text{Fe}^{3+}$  and  $\text{Ti}^{4+}$  do in combination, which aligns with Kumar et al.'s (2020)[7] observations of relatively lower dielectric constants and larger crystallite sizes in Cr-doped alumina.

In conclusion, the study demonstrates that  $\text{Fe}_2\text{O}_3+\text{TiO}_2$  is a more effective dopant than Cr in enhancing the dielectric performance of alumina ceramics in the microwave frequency range.  $\text{Fe}_2\text{O}_3+\text{TiO}_2$ -doped alumina reaches a dielectric constant significantly higher than Cr-doped alumina. This enhancement correlates well with the FWHM data indicating smaller crystallite sizes and increased lattice strain for  $\text{Fe}_2\text{O}_3+\text{TiO}_2$ . The findings underscore the critical role of dopant selection and microstructural engineering in tuning the dielectric properties of ceramics, especially for high-frequency and resonant applications.

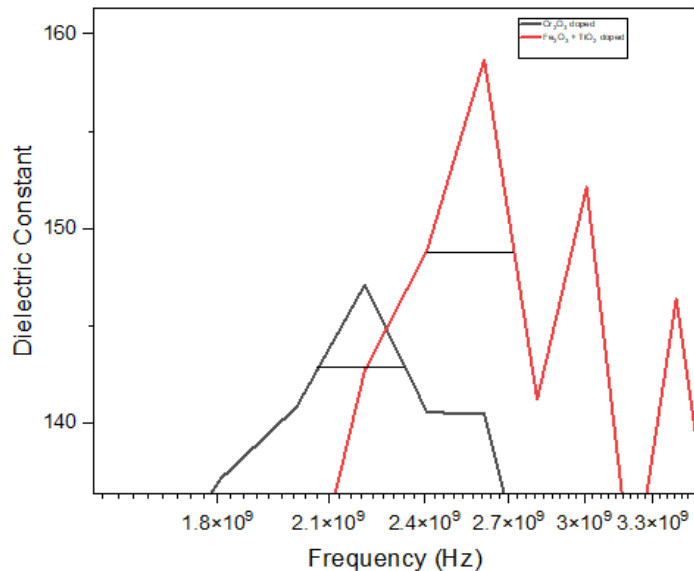


Fig. 26. FWHM of Chromium and  $\text{Fe}_2\text{O}_3+\text{TiO}_2$

The dielectric behavior observed in the graph reveals distinct frequency-dependent responses for pure and doped alumina systems, with each material exhibiting unique characteristics tied to specific polarization mechanisms and dopant effects. Pure  $\text{Al}_2\text{O}_3$  shows a stable dielectric constant ( $\epsilon'$ ) at low frequencies (up to ~0.04 GHz), consistent with the Maxwell-Wagner interfacial polarization model, where insulating grain boundaries dominate the dielectric response. This aligns with findings from Battat et al. (2007)[7], who demonstrated similar behavior in  $\text{Al}_2\text{O}_3-\text{SiC}$  composites. Beyond this range,  $\epsilon'$  gradually declines due to the inability

of dipoles to align with high-frequency fields, while a sharp relaxation peak at 1.8 GHz suggests dipole reorientation. The loss tangent ( $\tan \delta$ ) remains low initially but rises sharply above 0.01 GHz, indicating increased conductive losses at higher frequencies.

Vanadium-doped  $\text{Al}_2\text{O}_3$  exhibits enhanced  $\epsilon'$  values and improved stability at higher frequencies, with the relaxation peak at 1.8 GHz broadening significantly. This behavior mirrors studies on  $\text{V}_2\text{O}_5$ -doped systems, where vanadium incorporation modifies grain boundary resistance and suppresses dipole polarization, leading to better high-frequency performance. The shift in  $\tan \delta$  stability to 0.08 - 1.10 GHz further reflects the dopant's role in altering charge carrier dynamics. In contrast,  $\text{Fe}_2\text{O}_3$ -doped  $\text{Al}_2\text{O}_3$  displays a substantial rise in  $\epsilon'$  at low frequencies, attributed to the Maxwell-Wagner-Sillars effect, where conductive  $\text{Fe}_2\text{O}_3$  nanoparticles form micro capacitor networks, enhancing interfacial polarization. This phenomenon is well-documented in studies, where percolation effects dominate at higher dopant concentrations. The steep decline in  $\epsilon'$  at higher frequencies and elevated  $\tan \delta$  at lower frequencies underscore the conductive nature of  $\text{Fe}_2\text{O}_3$ -doped systems.

For the  $\text{Fe}_2\text{O}_3 + \text{TiO}_2$  doped alumina sample, the quality factor (Q-factor) loaded was calculated using the formula  $Q = f_0 / \Delta f$ , where  $f_0 = 158.66$  Hz is the resonance frequency and  $\Delta f = 55$  Hz is the bandwidth. The resulting Q-factor is 2.88, indicating the sharpness of resonance observed during VNA measurement.

Minor variations in dopant concentration critically influence relaxation peaks and loss thresholds, highlighting the sensitivity of dielectric properties to compositional changes. These findings demonstrate how vanadium doping optimizes alumina for high-frequency stability by modifying grain boundaries, while  $\text{Fe}_2\text{O}_3$  doping enhances low-frequency permittivity through conductive network formation. Such tailored dielectric responses make these materials suitable for diverse applications, from low-loss microwave ceramics to high-capacitance systems, with performance directly linked to dopant-induced microstructural modifications.

Table 9. Highest peak frequency and FWHM of samples

Dopant added(0.2 wt%)	Frequency(Hz)	FWHM
Pure Alumina	$2.2 \times 10^9$	$1.23 \times 10^{10}$
$\text{Cr}_2\text{O}_3$ doped	$2.2 \times 10^9$	$1.04 \times 10^{10}$
$\text{V}_2\text{O}_5$ doped	$2.6 \times 10^9$	$1.036 \times 10^{10}$
$\text{Fe}_2\text{O}_3$ doped	$1.2 \times 10^9$	$1.12 \times 10^{10}$
$\text{Fe}_2\text{O}_3 + \text{TiO}_2$ doped	$2.6 \times 10^9$	$1.18 \times 10^{10}$

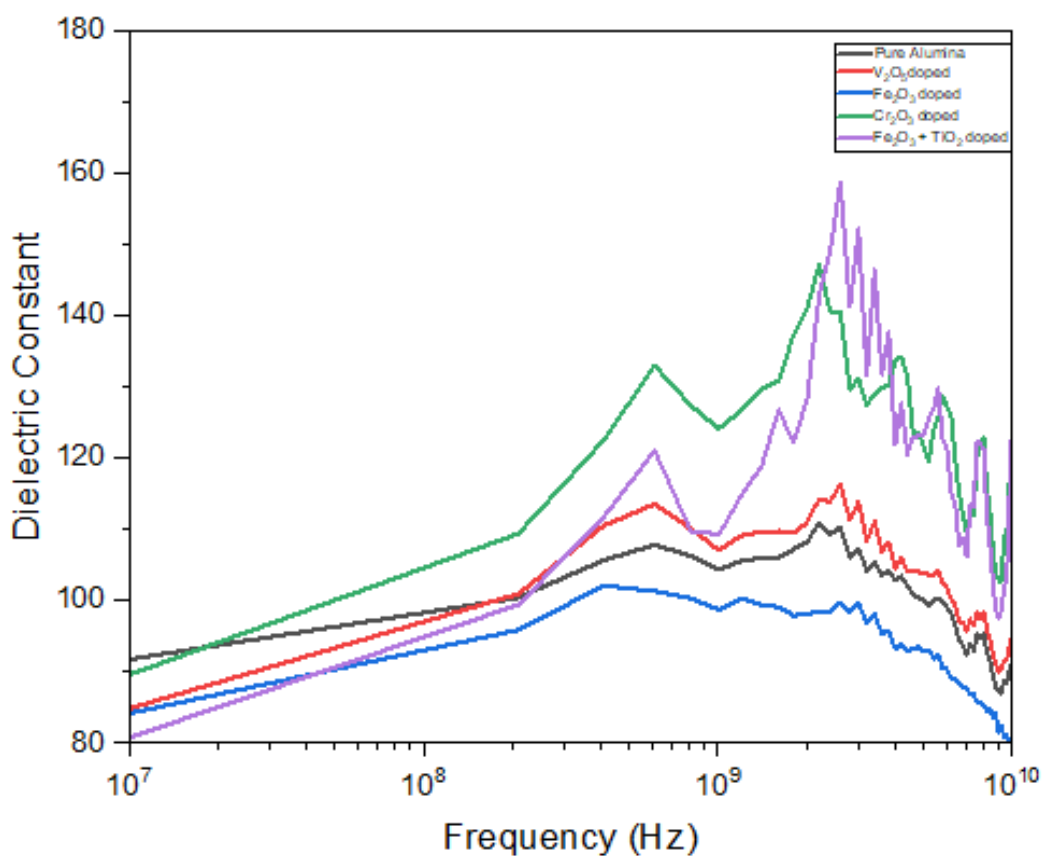


Fig.27. Dielectric Constant Vs Frequency [Hz] [VNA]

#### 4.2.5 Dielectric Loss – VNA

The dielectric loss versus frequency graph for various doped alumina samples in the range of 2–10 GHz reveals important insights into their behavior in microwave frequency applications, particularly around 4 GHz, which falls within the S and C band spectrum commonly used in radar and satellite communication. At this frequency, the dielectric loss values for different compositions show a clear trend. Chromium-doped alumina exhibits the highest dielectric loss of 22.22, followed by the  $\text{Fe}_2\text{O}_3 + \text{TiO}_2$  combination at 20.37,  $\text{V}_2\text{O}_5$ -doped alumina at 19.04, pure alumina at 18.70, and  $\text{Fe}_2\text{O}_3$ -doped alumina at 17.39, the lowest among all.

The high loss in Cr-doped alumina is attributed to the significant lattice distortion caused by  $\text{Cr}^{3+}$  ions, which introduce a large number of structural defects. These defects promote space charge polarization and increase dielectric relaxation losses due to the trapping and release of charge carriers under alternating electric fields. In the case of  $\text{Fe}_2\text{O}_3 + \text{TiO}_2$ , the presence of mixed valence states ( $\text{Fe}^{3+}/\text{Fe}^{2+}$  and  $\text{Ti}^{4+}/\text{Ti}^{3+}$ ) enhances electron hopping across localized states, resulting in strong interfacial polarization. However, this also leads to increased dielectric losses due to conduction and defect-related relaxation mechanisms.

Vanadium-doped alumina shows a slightly lower dielectric loss compared to Cr and Fe-Ti systems, primarily because of controlled electron hopping between  $\text{V}^{5+}$  and  $\text{V}^{4+}$  states. This hopping contributes to space charge polarization but does not severely disrupt the crystal lattice, thus limiting excessive dielectric loss. Pure alumina, which lacks significant mobile charge carriers, exhibits dielectric loss mainly due to ionic and electronic polarization, with minimal contribution from conduction losses. This results in a relatively low and stable loss profile.

Interestingly,  $\text{Fe}_2\text{O}_3$ -doped alumina demonstrates the most favorable behavior with the lowest dielectric loss. This is due to moderate electron hopping and minimal structural damage, which preserves the grain boundary resistance and prevents the formation of conductive paths. As a result, dielectric relaxation remains low, making this composition highly suitable for microwave frequency applications. The overall trend in the graph also shows that all samples exhibit increasing dielectric loss with frequency, which is a typical behavior due to the lag of polarization mechanisms—especially dipolar and interfacial—with increasing electric field oscillation. At higher frequencies, the polarization mechanisms cannot follow the field variation effectively, resulting in energy dissipation in the form of dielectric loss.

In conclusion,  $\text{Fe}_2\text{O}_3$ -doped alumina offers the most stable and low-loss performance at 4 GHz,

making it the best candidate for applications in the S and C bands, followed by pure alumina and vanadium-doped alumina. In contrast, chromium and  $\text{Fe}_2\text{O}_3 + \text{TiO}_2$  doped samples exhibit higher dielectric losses due to enhanced defect-related polarization and conduction effects.

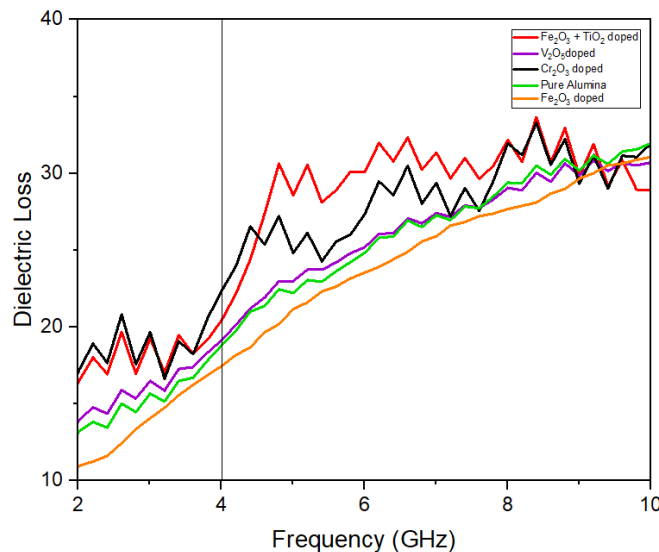


Fig.28. Dielectric Loss Vs Frequency [VNA]

Table 10 .  $\epsilon'$ ,  $\epsilon''$ ,  $\tan \delta$ , Quality factor(loaderd) values

COMPOSITION	$\epsilon'$	$\epsilon''$	TAN DELTA	QUALITY FACTOR(LOADED)
Pure Alumina	102.90	18.70	0.186	2.99
Cr <sub>2</sub> O <sub>3</sub> doped	133.55	22.22	0.186	3.9
V <sub>2</sub> O <sub>5</sub> doped	104.70	19.04	0.187	3.4
Fe <sub>2</sub> O <sub>3</sub> doped	93.30	17.39	0.181	5.1
Fe <sub>2</sub> O <sub>3</sub> +TiO <sub>2</sub> doped	122.30	20.37	0.200	2.88

### 4.3 Hardness test

To assess the influence of dopants and sintering cycles on the mechanical properties of alumina ceramics, Rockwell Superficial Hardness testing was conducted on five different compositions:

- Pure Alumina ( $\text{Al}_2\text{O}_3$ )
- $\text{Al}_2\text{O}_3 + \text{Fe}_2\text{O}_3$

- $\text{Al}_2\text{O}_3 + \text{Cr}_2\text{O}_3$
- $\text{Al}_2\text{O}_3 + \text{Fe}_2\text{O}_3 + \text{TiO}_2$  (co-doped)
- $\text{Al}_2\text{O}_3 + \text{V}_2\text{O}_5$

Each material group underwent three sintering cycles. For each group, three indentations were taken, and the average hardness was calculated. The results were plotted as individual bar charts for each sintering cycle, using color-coded bars to distinguish between different compositions.

### **Graph 1: 1st Sintering Cycle**

- Pure Alumina recorded the highest average hardness (~89 HR), showcasing its inherent mechanical robustness.
- Fe-doped alumina followed closely (~81 HR), benefiting from strong grain boundary strengthening due to  $\text{Fe}^{3+}$  ion substitution.
- Cr-doped alumina showed consistent hardness (~77 HR), attributable to its well-known ability to enhance grain boundary cohesion.
- Fe + Ti co-doped alumina had lower hardness (~55 HR), indicating incomplete densification or weaker grain interface development in a single sintering cycle.
- $\text{V}_2\text{O}_5$ -doped alumina recorded the lowest (~21 HR), likely due to porosity and underdeveloped microstructure caused by low-temperature liquid phase sintering in early stages.

### **Graph 2: 2nd Sintering Cycle**

Across all compositions, hardness values increased noticeably, indicating improved densification and grain bonding with a second thermal cycle.

- Pure alumina increased to ~96 HR, confirming enhanced grain packing.
- Fe + Ti showed the most dramatic jump (~84 HR from 55 HR), suggesting synergistic densification from dual dopants becoming effective after re-sintering.
- Cr and Fe doped samples crossed ~84–86 HR, showing more uniform microstructure and better mechanical load distribution.
- $\text{V}_2\text{O}_5$ -doped samples improved significantly (~52 HR), although still lower than other compositions due to retained porosity.

### **Graph 3: 3rd Sintering Cycle**

The third sintering cycle showed a plateau or saturation effect for most materials, indicating the microstructure had nearly reached its peak density and hardness.

- Pure Alumina achieved maximum average hardness (~98 HR), confirming exceptional densification and minimal defect density.
- Fe-doped and Cr-doped samples stabilized at ~91–93 HR, showing the consistent contribution of these dopants to mechanical reinforcement.
- Fe + Ti reached ~91 HR, demonstrating that co-doping is highly effective in multi-cycle sintering regimes.
- V<sub>2</sub>O<sub>5</sub>, while still the lowest (~60 HR), continued to show improvement, possibly due to elimination of residual pores and completion of phase stabilization.

#### **Impact of Repeated Sintering:**

Each additional sintering cycle improved hardness by:

- Reducing internal pores
- Enhancing grain boundary bonding
- Completing secondary phase transformations
- Promoting uniform grain structure

#### **• Dopant Effects:**

- Fe<sub>2</sub>O<sub>3</sub> and Cr<sub>2</sub>O<sub>3</sub> effectively strengthen grain interfaces and promote densification, yielding consistent hardness across cycles.
- Fe + Ti co-doping benefits from synergy; Ti<sup>4+</sup> supports grain refinement, while Fe<sup>3+</sup> improves diffusion, especially visible after the second and third cycles.
- V<sub>2</sub>O<sub>5</sub>, although less mechanically reinforcing, shows gradual gains likely due to the formation of vanadate phases and pore closure.

#### **• Microstructural Correlation:**

Hardness increases are typically associated with:

- Smaller, more uniform grains
- Elimination of intergranular voids
- Stronger ionic bonding due to dopant incorporation

Table 11. Hardness values of each sintering cycle(Superfacial Rockwell machine(HR))

Dopant	1st Cycle	2nd Cycle	3rd Cycle
Pure Alumina	89.3	96	97.7
Cr <sub>2</sub> O <sub>3</sub> doped	54.7	83.7	91.3
V <sub>2</sub> O <sub>5</sub> doped	76.7	77.3	87.0
Fe <sub>2</sub> O <sub>3</sub> doped	81.3	89.0	91.0
Fe <sub>2</sub> O <sub>3</sub> +TiO <sub>2</sub> doped	50.5	52	60

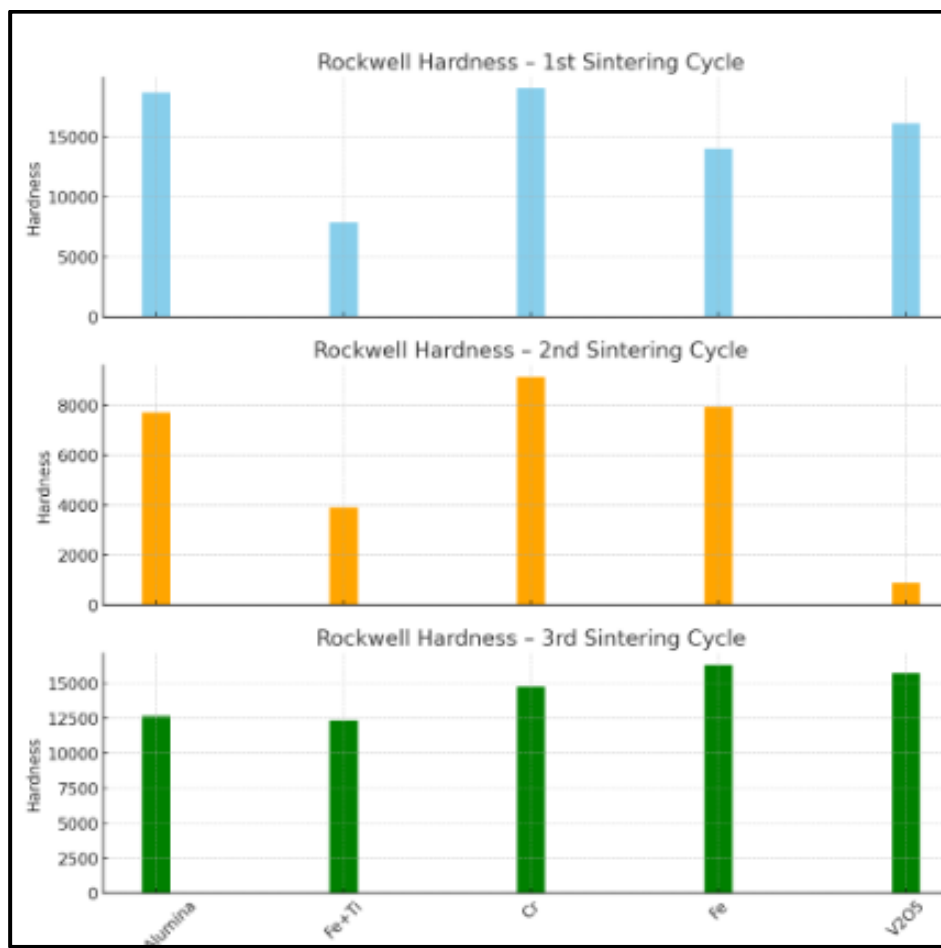


Fig.29. Hardness Analysis

#### 4.4 Compression test

The compression test results reveal a clear influence of dopant type and sintering cycle on the mechanical behavior of the alumina-based samples. In the first sintering cycle, the highest compressive strength was observed in the  $\text{Cr}_2\text{O}_3$  doped sample (19000 N), followed by  $\text{V}_2\text{O}_5$  doped (16105 N) and pure alumina (18645 N), indicating that initial densification and grain boundary pinning by dopants contribute significantly to strength.

By the third sintering cycle, a recovery in strength was evident across most samples, with  $\text{Fe}_2\text{O}_3$  doped alumina reaching the highest value (16328 N), potentially due to improved densification or phase transformation during repeated sintering.  $\text{V}_2\text{O}_5$  and  $\text{Cr}_2\text{O}_3$  doped samples also showed improved strength compared to the second cycle, indicating partial healing of microstructural defects or further densification.

Overall,  $\text{Cr}_2\text{O}_3$  doped alumina demonstrated consistently high performance across all cycles, while  $\text{Fe}_2\text{O}_3$  doped samples showed significant strength recovery after the third cycle.

Table 12. Peak Load(N) values for each sintering cycle

Composition	1st Sintering Cycle (N)	3rd Sintering Cycle (N)
Pure Alumina	18645	12649
$\text{Cr}_2\text{O}_3$ doped	19000	14741
$\text{Fe}_2\text{O}_3 + \text{TiO}_2$ doped	7824	12347
$\text{V}_2\text{O}_5$ doped	16105	15687
$\text{Fe}_2\text{O}_3$ doped	14000	16328

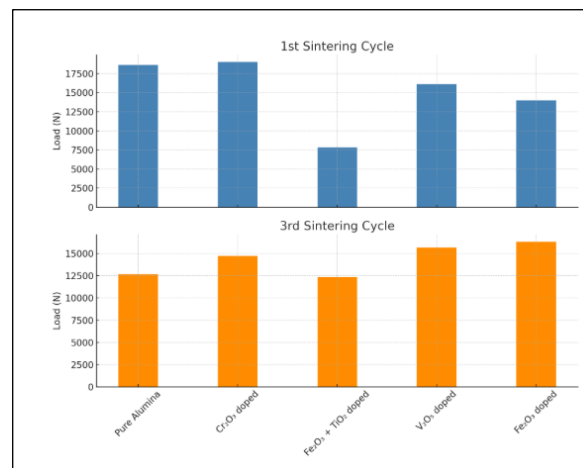


Fig 30. Compression Analysis

## **CHAPTER - 5**

### **CONCLUSION**

This project demonstrated that doping alumina ( $\text{Al}_2\text{O}_3$ ) with transition metal oxides— $\text{Fe}_2\text{O}_3$ ,  $\text{Fe}_2\text{O}_3 + \text{TiO}_2$ ,  $\text{Cr}_2\text{O}_3$ , and  $\text{V}_2\text{O}_5$ —can significantly enhance its performance for microwave dielectric resonator applications. XRD analysis confirmed that  $\text{Cr}^{3+}$  substitutes well into the  $\text{Al}_2\text{O}_3$  lattice without forming secondary phases.

Dielectric testing using impedance spectroscopy and VNA showed that all samples exhibit frequency-dependent behavior with decreasing dielectric constant ( $\epsilon'$ ) and loss ( $\tan \delta$ ) at higher frequencies. At 4 GHz (S and C band),  $\text{Fe}_2\text{O}_3$ -doped alumina showed the lowest dielectric loss (17.39), making it most suitable for microwave applications.  $\text{Cr}_2\text{O}_3$ -doped samples showed the highest loss (22.22), while Fe-Ti and  $\text{V}_2\text{O}_5$  samples exhibited moderate performance.

Mechanically,  $\text{Fe}_2\text{O}_3$  and pure alumina displayed the highest hardness values (~93–98 HR) after three sintering cycles, indicating excellent densification.  $\text{V}_2\text{O}_5$ -doped samples remained the softest due to porosity. Overall,  $\text{Fe}_2\text{O}_3$ -doped alumina with triple sintering offered the best combination of low dielectric loss, good dielectric constant, and high mechanical strength—making it the most promising material for high-frequency, low-loss microwave dielectric resonators.

The study highlights the significant role of dopant selection and sintering cycles in enhancing the compressive strength of alumina-based ceramics.  $\text{Cr}_2\text{O}_3$  doping consistently provided high mechanical performance, indicating its effectiveness in strengthening mechanisms such as grain boundary pinning. Meanwhile,  $\text{Fe}_2\text{O}_3$  doping, despite its lower initial strength, exhibited remarkable improvement after repeated sintering, likely due to enhanced densification or phase evolution. These findings suggest that both  $\text{Cr}_2\text{O}_3$  and  $\text{Fe}_2\text{O}_3$  are promising dopants for optimizing the mechanical reliability of alumina ceramics through tailored thermal processing.

## FUTURE SCOPE

- Detailed Microstructural Analysis using high-resolution FESEM and TEM can provide deeper insights into grain boundaries, porosity, and dopant distribution.
- Refining dopant levels in smaller steps may help further improve dielectric and structural properties.
- Advanced Sintering Techniques like spark plasma sintering (SPS) or microwave sintering can enhance densification and reduce energy usage.
- Thermal Stability and Cycling Tests can assess long-term performance under operating conditions.
- Testing doped alumina in real microwave circuits can validate its practical application.
- Unloaded quality factor is to be determined.
- Temperature of samples needs to be verified to know the temperature coefficient of dielectric constant, conductivity and band gap.

## REFERENCES

1. Dong Zhao,Fa Luo, Wancheng Zhou, and Dongmei Zhu. 2013. International journal of applied ceramic technology.10 [S1] E88–E97.Complex Permittivity and Microwave-Absorbing Properties of Fe/Al<sub>2</sub>O<sub>3</sub> Coatings by Air Plasma Spraying Technique
2. R. Umashankar Rajab, H.C. Manjunatha,c, Y.S. Vidyad. 2024. Chemical Physics Impact. 9 (2024) 100710. The structural, magnetic and electrical properties of chromium doped calcium ferrite nanoparticles.
3. D. Di Marcoa, K. Drissib, N. Delhote.2016. Journal of the European Ceramic Society. 36 (2016) 3355–3361. Dielectric properties of pure alumina from 8 GHz to 73 GHz.
4. osites Kaleem Ahmad, Wei Pan, and Sui-Lin Shi . 2006. Appl. Phys. Lett.. 89, Electrical conductivity and dielectric properties of multiwalled carbon nanotube and alumina composites.
5. Sanjeet Kumar Paswan. 2022. Phys. Scr. 97 095812. Electrical transport properties of nanocrystalline and bulk nickel ferrite using complex impedance spectroscopy: a comparative study.
6. DEBASIS ROY, PARVEEN SULTANA,SUBHAJIT GHOSH.2012. Bull. Mater. Sci., Vol. 36,Electrical and dielectric properties of TiO<sub>2</sub> and Fe<sub>2</sub>O<sub>3</sub> doped fly ash.
7. Jin Soo Kim.1998. Molecules,24.Dielectric and Piezoelectric Properties of Fe<sub>2</sub>O<sub>3</sub>-doped 0.57PSN-0.43PT Ceramics.
8. J. Battata and J.P. Calame. 2007. Journal of korean physical society,32. Analysis of the complex dielectric permittivity behavior of porous Al<sub>2</sub>O<sub>3</sub>–SiC composites in the 1 MHz to 18 GHz frequency range.
9. Cheng-Liang Huangw and Jun-Jie Wang.2007. Current Applied Physics22.Microwave Dielectric Properties of Sintered Alumina Using Nano Scaled Powders of Alpha Alumina and TiO<sub>2</sub>.
10. Cheng-Liang Huang a, Jun-Jie Wang a, Chi-Yuen Huang b.2005.Sintering behavior and microwave dielectric properties of nano alpha-alumina.
11. Dipti Patnaik, Praveen P. Nayak, S. Bhuyan, S.N. Das. 2023. Naval Research Laboratory, Washington, DC 20375.Temperature and frequency dependent dielectric and electrical properties of relaxor (Ca1/2W1/2)(Pb1/2Ni1/2)O<sub>3</sub> electronic material.
12. Ranjan Bhuyan, Santhosh Kumar,John Renahan,Mohan Jacob. 2014. Low temperature and broadband dielectric properties of V<sub>2</sub>O<sub>5</sub> doped Mg<sub>2</sub>TiO<sub>4</sub> ceramics.
13. S Ahmed Farag, I K Battisha. 2005.J.Am ceramic society,90 Study of dielectric properties of Alumina doped with MnO,CdO and MoO.
14. Anand K Tyagi, Parul. 2014. Materials letter,90.Synthesis and characterization of ceramic dielectric resonator materials for microwave communication technology.
15. T. Kolodiaznyia,\* G. Annino. 2009. Results in Chemistry5. Development of Al<sub>2</sub>O<sub>3</sub>–TiO<sub>2</sub> composite ceramics for high-power millimeter-wave application.

## **ACKNOWLEDGMENT**

We are indebted to our project guide Dr. S.P.Butee Sir for his valuable suggestions and motivation that he provided us. He has been a source of constant inspiration and generous assistance during the project work. We thank his kindness in helping us to make use of all facilities available in the department. The entire course of our project has been a period of learning and experiencing the new technologies available. It has helped us to increase our persistence and determination levels and lead us to continue the research further. We are thankful to HoD Dr. M.G. Kulthe Ma'am, Head of Department, and other staff members for encouraging us all the time and giving their suggestions.

Finally, we express our gratitude to all who have helped us directly or indirectly during the course of the project.